Spring 2022

Classification of Acoustic Emission Data Into Load Steps Using An Artificial Neural Network

Allen Ross

CLASSIFICATION OF ACOUSTIC EMISSION DATA INTO LOAD STEPS USING AN ARTIFICIAL NEURAL NETWORK

by

Allen Ross

Bachelor of Science
University of South Carolina, 2021

Submitted in Partial Fulfillment of the Requirements

For the Degree of Master of Science in

Civil Engineering

College of Engineering and Computing

University of South Carolina

2022

Accepted by:

Paul Ziehl, Director of Thesis

Bin Zhang, Reader

Sarah Gassman, Reader

Tracey L. Weldon, Interim Vice Provost and Dean of the Graduate School

DEDICATION

To my mom and dad, the ones that love and support me endlessly and unconditionally. To Kathleen, Sarah, and John the ones whose exceptionality is not only an inspiration but the standard that I strive to hold myself to every day.

ACKNOWLEDGEMENTS

This body of work is the culmination of contributions made by many different people, both directly and indirectly. I would firstly like to thank my supervisor Dr. Paul Ziehl at the University of South Carolina. With his support I was able to compete in a collegiate sport and graduate with an advanced degree in engineering. He has been an incredible example of a man within the industry, and I hope one day I may know half as many things as he knows.

I would also like to thank my research team Dr. Li Ai, Laxman K C, Elhussien Elbatanouny, Alex Henderson, and Dr. Mahmoud Bayat. All of whom contributed greatly to this body of work and without whom I would be lost.

I would like to thank my committee members, Dr. Sarah Gassman and Dr. Bin Zhang, for their support throughout my research and for serving on my committee.

I would like to thank my family, friends, coaches, and team for supporting me while I studied. Many of them have had a direct impact on this body of work.

I would like to thank the University of South Carolina for giving me the opportunity to further my education.

Lastly, I would like to thank God for blessing me with these people who have made time for me and allowed me to accomplish something greater than myself.

ABSTRACT

The average age of bridges in South Carolina is approaching 40 years, very close to the 50-year service life. Almost 11% of the bridges in South Carolina are rated as structurally deficient, greater than the national average of 7.5% (South 2021). Health monitoring is the concept that in-situ sensors can continuously monitor civil structures and send real time signals of damage. This process allows for automation and could save time and money on the inspection and load rating of bridges. Health monitoring requires sensors that provide uninterrupted data without sacrificing the functionality of the bridge. A prime candidate for this is acoustic emissions data which can gather information on an entire bridge with a few small sensors.

This study focuses on the classification of acoustic emission (AE) data using an artificial neural network (ANN) in hopes that it will contribute to the advancement in structural health monitoring (SHM) procedures for precast reinforced concrete flat slab superstructures. In addition, it will focus on the viability of acoustic emission data for health monitoring systems as well as the practicality of artificial neural networks on the classification of this data.

In addition, AE signals are analyzed and classified into load steps using statistical methods and an ANN. The statistical analysis provided slight differences between load steps, but classification proved difficult using a single feature of an AE waveform. The ANN was much more successful in classification of the AE data into

2 different load steps. The trained ANN was able to classify an unfamiliar data set. with 73.0% accuracy.

TABLE OF CONTENTS

LIST OF TABLES

LIST OF FIGURES

LIST OF SYMBOLS

f'_c	Compressive strength of concrete.
f_y	Yield strength of steel.
L	Length of slab.
E	Width of slab.
D	Depth of slab.
W	Width of bearing.
a	Length of bearing pad.
b	Width of bearing pad.
c	Distance from center to center from one bearing pad to the other.
d	Width of the spreader beam.
F	Length of spreader beam.
X	Shear span length
μ	Mean.
σ	Standard deviation.
$P_A(x)$	Probability of x amplitude.
λ	Rate parameter.

LIST OF ABBREVIATIONS

AE ..... Acoustic Emission

ANN ..... Artificial Neural Network

SHM ..... Structural Health Monitoring

SCDOT ..... South Carolina Department of Transportation

DIC ..... Digital Image Correlation

TRC ..... Textile Reinforced Concrete

CFRP ..... Carbon Fiber Reinforced Polymer

UHPC ..... Ultra High-Performance Concrete

AI ..... Artificial Intelligence

CNN ..... Convolution Neural Network

ABS ..... Acrylonitrile-butadiene-styrene

UHMWPE/LDPE ..... Ultra-High Molecular Weight Polyethylene Fiber Reinforced Low Density Polyethylene Composites

UPR ..... Unsupervised Pattern Recognition

SPR ..... Supervised Pattern Recognition

SEM ..... Scanning Electron Microscope

BPNN ..... Back Propagation Neural Network

SAE ..... Sparse Autoencoder

PDF ..... Probability Density Function

T1 ..... Test 1

T1L1 ..... Test 1 Load step 1

T1L2 ..... Test 1 Load step 2

T1L3 ..... Test 1 Load step 3

T2 ..... Test 2

T2L1 ..... Test 2 Load step 1

T2L2 ..... Test 2 Load step 2

T2L3 ..... Test 2 Load step 3

CHAPTER 1

INTRODUCTION

1.1 Description of Problem

The average age of bridges in South Carolina is approaching 40 years, very close to the 50-year service life. Almost 11% of the bridges in South Carolina are rated as structurally deficient, greater than the national average of 7.5% (South 2021). After many years of neglect, the US has decided to put infrastructure in the front seat. The state of South Carolina recognizes the importance of functional infrastructure, especially for its bridges. South Carolina has 9,455 bridges in its inventory, many of which were designed using either H-10 or H-15 loading criteria. H-10 refers to a two-axel truck weighing 10 tons, or 20,000 pounds and H-15 is the same but for 15 tons, or 30,000 pounds. According to the South Carolina Department of Transportation (SCDOT), there are 3,622 bridges that were designed using these two loading criteria. The current design standard is called HL-93 which refers to a hypothetical 3 axle truck weighing in at 72 kips, or 144,000 pounds, and is significantly larger than the H-10 and H-15 loading criteria (AASHTO 2017). With over 30% of its bridges under-designed and suffering from decades of service deterioration, the SCDOT has made it a priority to evaluate these bridges and determine whether they need to be replaced or repaired. The typical methods of bridge evaluation are costly and time-consuming.

1.2 Cost of Evaluation

There are three different evaluation techniques used by South Carolina the first and most routine is called manual bridge inspection. Manual inspections usually occur biennially or, if deemed necessary, biannually. A bridge inspection is a 100% visual evaluation to determine the integrity of the bridge. It involves thorough note taking and photographs of every crack or other sign of deterioration. A typical bridge inspection utilizes 2-3 trained engineers for an entire day and usually requires traffic control. If every bridge in the SCDOT inventory was in good enough condition to be inspected biennially it would mean that an average of 20 bridges would need to be inspected per day. Because a bridge inspection is 100% visual, it can only detect and assess surface level issues. This means that a bridge inspection can only determine the surface level quality of the bridge and not the overall health or functionality.

A second, more in-depth, technique for evaluating the capacity of bridges is load rating. Load rating is the practice of using hand calculations to determine the ability of a structure to support certain vehicle loads. These calculations involve tracking down the original drawings of the structure and assuming that the bridge was built exactly to those drawings. There are a few issues with this method, one being that some of these bridge drawings are difficult if not impossible to track down, and the second being that often the drawings do not resemble the final product due to a miscommunication between the engineer and the contractor or an unintentional omission. Because of these issues, engineers are tasked with making assumptions about the bridges to finish these calculations and assumptions are inevitably conservative. Although hand calculations may not seem

like a significant cost, the computation and research time are significant. In fact, the SCDOT has dedicated over $120 million to the load rating efforts of the state.

The third evaluation technique, called diagnostic load rating, is used only if deemed necessary by the initial load rating effort. Diagnostic load rating occurs if the initial load rating suggests that it cannot support the required loading that the bridge may be subjected to. Diagnostic load rating requires a team of engineers to develop a computer model of the bridge and subject it to certain standardized loads while another team of engineers travels to the actual bridge and measures the physical responses of the real-world bridge to a known vehicle load. That information is then compared to the computer model and the digital model is recalibrated until it matches the real-world responses. Once a reliable computer model is developed, it can be used to determine responses to other vehicle loads. This method requires teams of engineers and traffic control and could span any number of days.

Each of these methods is costly and time-consuming; therefore, an accurate, more efficient evaluation method could save the state a substantial amount of money. This is where the idea of health monitoring comes in. Health monitoring is the concept that in-situ sensors can continuously monitor civil structures and send real time signals of damage (Brownjohn 2007). This process will allow for automation and could save time and money on inspections and load ratings or replace them all together. Health monitoring requires sensors that provide uninterrupted data without sacrificing the functionality of the bridge (Brownjohn 2007). A prime candidate for this is acoustic emissions data because of its ability to gather information on large proportions of a bridge with a few small sensors. This

thesis will focus on the evaluation of civil structures using acoustic emissions testing in hopes that it will contribute to the development of health monitoring of civil structures.

1.3 Acoustic Emission

Acoustic Emission (AE) has gained popularity in recent years through the recognition of its versatility. AE has been used as an evaluative tool for purposes ranging from the delamination of CFRP materials to the crispness and crunchiness of apples (Barile 2019, Zdunek et al. 2010). AE is defined as the transient elastic waves within a material, caused by the rapid release of localized strain energy (Ai et al. 2021). Simply put, and in the context of this thesis, AE is used to describe particular sensor responses that are caused by stress waves associated with a number of sources, including crack initiation and extension (other definitions may be found in literature, such as Scruby 1987). As micro or macro cracks occur within a structure, AE sensors respond to out of surface displacements caused by stress waves. The recording of a particular signal is referred to as a "hit". The sensor response is in the form of a wave. A typical AE waveform associated with a hit is shown in Figure 1.1. A waveform has many different attributes that allow researchers to categorize each hit. The categorization and classification of AE hits has been a subject of discussion since the development of the technology. Classification of data points is necessary to interpret and gather meaningful insights from the data. Problematically, it is somewhat difficult to classify data points with AE due to the similarities between waveforms gathered under separate loading conditions and the sheer number of hits generated during testing. AE waveforms collected under totally separate loading or unloading conditions may have similar attributes or look very similar to one another, which poses a challenge to the classification. Another challenge is the number of hits received

during a loading cycle. Depending on the load, thousands, if not tens of thousands, of AE hits may be received. To address these two challenges an Artificial Neural Network was used for this thesis.

1.4 Artificial Neural Network

An Artificial Neural Network (ANN) is a computing system inspired by biological neural networks. It is composed of an input layer, a series of hidden layers, and an output layer. Each layer contains many processing elements called neurons and each neuron is connected to others (Yang et al., 2004). An example of a 3-layer artificial neural network is shown in Figure 1.2.

The idea behind the model is motivated by the desire for a program to solve natural or intelligent tasks by leveraging advancements in computer technology (Yegnanarayana 2006). The model works like a biological brain when it comes to pattern recognition. Much like showing many pictures of dogs to a child and telling the child "Dog", then testing the child with a collection of pictures of different animals confirms that the child has learned the differences. The same is true for an ANN. The network is trained with data points and then told the "rules" of classification. The training of the neural network can be compared to the homework stage of a class where the network is learning how to classify these data points. After training, the network is validated. The validation stage can be compared to the quizzes in the class where the network is tested but the overall grade of the network is not affected by the results of the quiz. The network is then tested for accuracy. The testing stage is compared to the final exam of a class where the network truly tested, and the results of an incorrect classification will affect the reliability of the model.

In this thesis the ANN used was trained, validated, and tested on a specific set of data collected from one specimen and then, once trained and validated, it was tested on a set of data collected from different specimen to see the consistency and reliability of this method of classification.

1.4 Specimen Tested

For this thesis, precast reinforced concrete flat slab superstructures were investigated. These components were selected due to their prevalence in the bridge inventory and the widespread need for evaluation of these types of structures in South Carolina.

1.5 Objectives

The investigations addressed in this thesis are intended to contribute to the development of health monitoring systems. This thesis will focus on the viability of acoustic emission data for a health monitoring system on precast reinforced concrete flat slab superstructures. More specifically this thesis will develop a method for classifying AE data based on load steps. This will contribute to SHM because it has the potential to identify damage of a structure in real time.

Specific goals of the project include:

- Identification of AE hit attributes collected from different load steps.
- Classification of AE hits to different load steps.
- Development of an ANN that can quickly and effectively classify AE data.
- Behavior of structure under typical truck axle loads.

These goals are addressed through experimental, analytical, and computational methods.

1.6 Layout of Thesis

This thesis is composed of 5 chapters. Chapter 2 is a literature review of the different classification methods for AE. In Chapter 3 the specific methodologies of the experiment are presented. Findings of the study are presented in Chapter 4 followed by a discussion of the findings presented in Chapter 5. Chapter 5 also includes the recommendation for future studies on this topic.

1.7 Figures

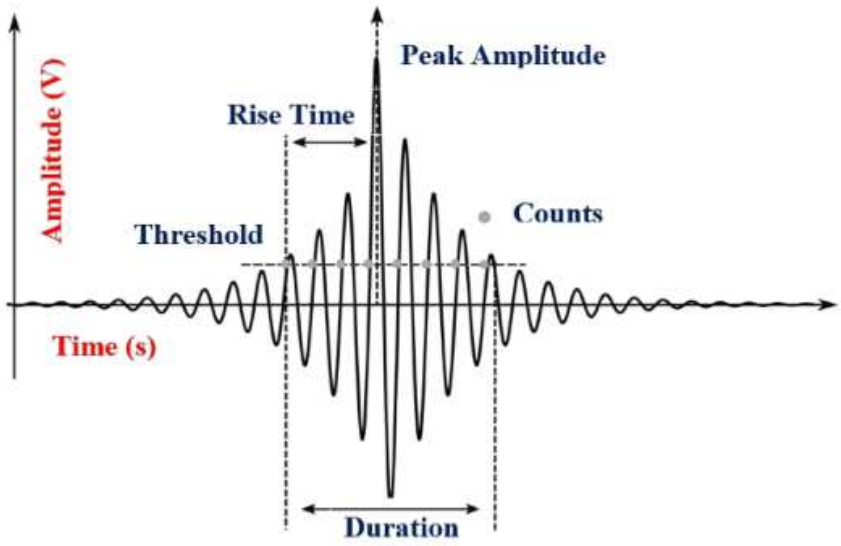

Figure 1.1 Illustration of a typical acoustic emission hit (Li et al. 2021)

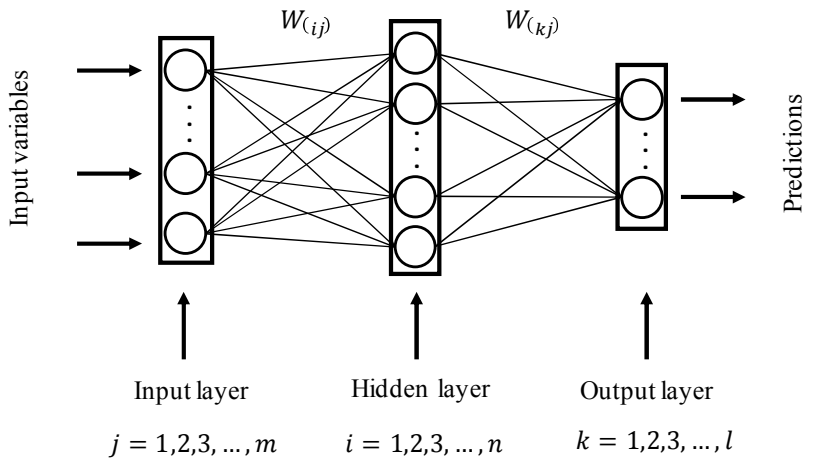

Figure 1.2 Example of a 3-layer ANN (Li et al. 2021)

1.8 References

AASHTO (2017). Bridge design specifications. American Association of State Highway and Transportation Officials, AASHTO: Washington, DC, USA.

Ai, L., Soltangharaei, V., Bayat, M., Greer, B., & Ziehl, P. (2021). Source localization on large-scale canisters for used nuclear fuel storage using optimal number of acoustic emission sensors. *Nuclear Engineering and Design*, *375*. https://doi.org/10.1016/j.nucengdes.2021.111097

Barile, C. (2019). Innovative mechanical characterization of CFRP by using acoustic emission technique. *Engineering Fracture Mechanics*, *210*. https://doi.org/10.1016/j.engfracmech.2018.02.024

Brownjohn, J. M. W. (2007). Structural health monitoring of civil infrastructure. *Philosophical Transactions of the Royal Society A: Mathematical, Physical and Engineering Sciences*, *365*(1851). https://doi.org/10.1098/rsta.2006.1925.

Gifford, J. L. (1984). The innovation of the interstate highway system. *Transportation Research Part A: General*, *18*(4). https://doi.org/10.1016/0191-2607(84)90170-5Yegnanarayana, B. (2006). *Artificial Neural Networks*. Prentice-Hall of India.

Scruby, C. B. (1987). An introduction to acoustic emission. *Journal of Physics E: Scientific Instruments*, *20*(8). https://doi.org/10.1088/0022-3735/20/8/001

South Carolina: ASCE's 2021 infrastructure report card. ASCE's 2021 Infrastructure Report Card |. (2021, September 13). Retrieved March 11, 2022, from https://infrastructurereportcard.org/state-item/south-carolina/

Yang, S., & Browne, A. (2004). Neural network ensembles: combining multiple models for enhanced performance using a multistage approach. *Expert Systems*, *21*(5). https://doi.org/10.1111/j.1468-0394.2004.00285.x

Yegnanarayana, B. (2006). *Artificial Neural Networks*. Prentice-Hall of India.

Zdunek, A., Konopacka, D., & Jesionkowska, K. (2010). Crispness and crunchiness judgment of apples based on contact acoustic emission. *Journal of Texture Studies*, *41*(1). https://doi.org/10.1111/j.1745-4603.2009.00214.x

CHAPTER 2

LITERATURE REVIEW

2.1 Concrete AE Evaluation

Acoustic emission monitoring for assessment of prestressed concrete beams

Elbatanouny et al. (2014) investigated the monitoring abilities of AE on eight prestressed concrete T-beams subjected to cyclic load testing. The beams were 16'4" in length and 3 beams were left uncracked, 4 beams were pre-cracked with a maximum crack width of approximately 0.016 in. and one beam was pre-cracked with a maximum crack width of approximately 0.032 in. Two of the beams had pre-corroded strands to investigate the effect of corrosion on AE data. The experimental setup can be seen in figure 2.1.

Using the AE data, the authors were able to gather conclusions from an intensity analysis, the relaxation ratio, and the b-value analysis. "Intensity Analysis is performed by calculating the historic index and severity from signal strength" (Elbatanouny et al. 2014). The historic index and severity were calculated using equations (2.a) and (2.b), respectively.

$$H(t) = \frac{N}{N-K}\frac{\sum_{i=K+1}^{N} S_{oi}}{\sum_{i=1}^{N} S_{oi}} \quad (2.a)$$

$$S_r = \frac{1}{50}\sum_{i=1}^{i=50} S_{oi} \quad (2.b)$$

Intensity analysis was performed for all specimens only using the AE data collected from sensor 9. This approach was taken because it seemed like the most reasonable

representation of what a real-world analysis would look like. The authors of the paper developed intensity analysis charts and this method was successful in quantifying the existing damage to the beams.

The relaxation ratio method was conducted by taking the average AE energy during unloading and dividing it by the average AE energy during loading. This method helps in determining crack propagation because, in prestressed beams, AE energy during unloading increases as cracks begin to form because of crack closure and friction between the surfaces of the cracks. Elbatanouny et al. (2014) concluded that the relaxation ratio analysis can detect crack initiation but only for the control specimen and not the pre-cracked specimen.

The b-value analysis is an empirically derived value "b" that is used as an indicator of the deterioration of a specimen due to cracking. From previous research it is known "that b-values under 1.0 correspond to the transition from micro-damage to macro-damage" (Elbatanouny et al. 2014). In this paper it was concluded that the b-value analysis was a good indicator of damage. The value showed damage a cycle before visible cracks formed on the control specimen and at the exact theoretical crack level for the pre-cracked specimen.

Using triangulation techniques, the authors of this paper were able to match the detected AE data with the visual cracks observed at the end of the test. According to this research-intensive data filtering is required prior to the source location. Figure 2.2(a) shows the unfiltered source location compared to Figure 2.2(c), which is the filtered version.

Although this testing was done on prestressed concrete beams the AE analysis methods can still be applied to reinforced concrete slabs.

Characterization of mechanical performance of concrete beams with external reinforcement by acoustic emission and digital image correlation

In Aggelis et al. (2013) the mechanical performance of externally reinforced concrete beams with acoustic emission and digital image correlation was measured. For this research four constructed beams underwent a four-point bending test. AE and digital image correlation (DIC) analyses were conducted for each beam. The external reinforcement on each of the beams varied. The first was reinforced by adding a high-performance textile reinforced concrete (TRC) layer to the entire bottom of the beam. The second was subjected to 40 kN of force to induce cracking and then it was reinforced with the same TRC technique. This was done to simulate conditions wherein reinforcement is added to a bridge after it has sustained prior damage. The third was reinforced with a carbon fiber reinforced polymer (CFRP) strip that was small enough to provide approximately the same reinforcement as the first beam. The last beam was left without reinforcement to provide a control.

There were eight different AE sensors on the center of the beams. Two types of sensors were used in the test: a resonant sensitive R15 sensor and a broadband WD sensor. The results were filtered by requiring a hit from at least 6 sensors within a certain amount of time to be classified as an AE event.

Aggelis et al. (2013) used the population of AE activity to determine the onset of cracking. Because ambient noise was minimal, the authors were able to use a low threshold which allowed them to collect more hits. It was noted that the externally reinforced beams

had a significantly lower amount of AE activity. The authors were able to use their sensors to determine the location of AE signals in 3-D space, which is different than other papers. The authors were also able to confirm, using AE signals, that crack propagation began at the bottom of the beam and moved vertically throughout the test. An attempt to identify possible fracture mechanisms through AE data analysis was made. The conclusion is that external reinforcement debonding "is connected to lower AE frequency and longer signal durations than the other mechanisms which certainly include matrix cracking or rebar yielding" (Aggelis et al. 2013). Furthermore, it was concluded that debonding AE hits does not contribute to the population before or after the load drops. The heterogeneity of concrete and the contribution that it has on the variability of AE waveforms was also discussed. Lastly, the paper vouches for the complimentary use of DIC, which allows for the minimization of assumptions during AE analysis.

Theoretical modelling and acoustic emission monitoring of RC beams strengthened with UHPC

In Prem et al. (2018) the authors applied AE sensors to damaged beams that were strengthened with ultra-high-performance concrete (UHPC) and tested them until failure. The goals of the test were analytical monitoring and acoustic emissions interpretation. The paper tested 9 different beams with varying reinforcement and thicknesses of UHPC strips. The beams were loaded to 90% of ultimate load to induce damage and then the UHPC was added to the beams. The beams were named for their rebar reinforcement and then the thickness of the UHPC strip. The number beside the letter coincided with the thickness of the UHPC strip. The number 1 meant the beam had a 10 mm thickness of UHPC, 2 meant a 15 mm thickness, and 3 meant a 20 mm thickness.

The beams were tested until failure using a four-point bending test (ASTM D6272) and AE data was collected throughout (ASTM. (2017). The authors first split the damage mechanisms into 5 zones or classifications. Zone I was correlated with no damage or elastic range, Zone II with hairline cracks, Zone III with visible cracks, Zone IV with crack formation in the retrofit strip, and Zone V with concrete crushing. The authors then conducted a "parametric analysis between moving average of the rise angle (RA) and average frequency (AF)" using equations (2.c) and (2.d).

$$RA = \frac{Rise\ Time}{Maximum\ Amplitude} \qquad 2.c$$

$$AF = \frac{Counts}{Duration} \qquad 2.d$$

Only AE analysis of the 15 mm thickness UHPC beams (A2, B2, and C2) was conducted because previous literature had determined it to be the optimum thickness for strengthening damaged beams. Once the analysis had been conducted, the authors were able to use the data to classify the type of crack formed using figure 2.8. Prem et al. (2018) also determined that most AE hits came from zone IV for A2 and B2 and zone V for C2. It was also determined that for all the beams, AF was greatest at Zone I. The data also shows that once the load carrying capacity of the tested beams drops, the AF value significantly decreases from the initial loading stage. The progression of damage also coincided with an increase in RA value. This research can be applied in the health monitoring of retrofitted structures.

2.2 ANN Classification

Neural network ensembles: combining multiple models for enhanced performance using a multistage approach

Yang et al. (2004) defines an ensemble ANN. The idea behind an ensemble is that by combining multiple models into a classification algorithm accuracy will be increase. According to this research, there are many ways to create an ensemble. The conventional ways are called simple averaging, weighted averaging, majority voting, and ranking. Yang et al. (2004) introduces the idea of creating a multistage neural network ensemble and tests it against majority voting because of the popularity of the combination method. Five different datasets with different numbers of input features and output features were used. It was concluded that ANN ensembles are more effective at achieving a higher accuracy rate than single nets. Moreover, multistage ANNs have a slightly better classification accuracy than majority voting. However, the complexity of a multistage ANN may outweigh the accuracy increase. In addition, variances were much smaller for ensemble results when using a multistage ANN versus a majority voting ANN.

Impact of Training Set Batch Size on the Performance of Convolutional Neural Networks for Diverse Datasets & Sample size requirements when using artificial neural networks for discrete

Radiuk (2018) discusses the effect of training batch size on the accuracy of image detection of a Convolutional Neural Network (CNN). While the increase in training size also increased accuracy, the computing time is a factor to be considered. Alwosheel et al. (2018) discusses the same concept using ANNs. It was concluded that the training data size of the network is dependent upon the complexity of the neural network structure. As the architecture of the neural network becomes more complicated the training sample size required for an accurate model increases. Alwosheel et al. (2018) also concludes that the optimization of the neural network is an iterative process, and only “rules of thumb” and basic estimations are provided.

Samples selection for artificial neural network training in preliminary structural design & Increasing the accuracy of neural network classification using refined training data

Tong et al. (2005) discussed the quantity and quality of training samples in preliminary structural design. Different models were built to determine the stability of K8-type dome shaped shells. With 6 inputs the models were asked to predict the critical load-capacity. In all, 3 different training sets, based on different numerical models, were used. It was concluded that the Hammersley-net was the optimal training set. Kavsoglu (2009) echoes the idea that both the quality and quantity of the training data set play an important role in the accuracy of the model. "The more representative samples introduced to a classification process, the more accurate and reliable results can be produced" (Kavsoglu 2009). Saxena (2006) also reiterates the importance of selecting the optimal feature set as well as the network complexity for ANNs.

2.3 AE Parameter Analysis

Acoustic emission - 2. Acoustic emission amplitudes

Analyses of the parameters of AE hits have been a topic of discussion for well over 40 years. In fact, Pollock (1973) conducted a distribution analysis of AE amplitude collected from 4 types of steel, two aluminum alloys, and a CFRP composite 49 years ago. He concluded that amplitude analysis may be useful in recognizing various deformation patterns and will most likely need to be paired with other processing methods to get a more complete picture of emission behavior.

Acoustic emission parameters and their interpretation

An in-depth analysis of the frequency, amplitude, and energy parameters were conducted in Stone (1977). The paper concludes that frequency content is heavily influenced by the resonances of the transducers and the specimens. It suggests that frequency alone has many conflicts that need to be resolved. This paper also agrees with Pollock (1973) that amplitude distribution can provide a way of distinguishing damage events.

Acoustic emission energy as a fatigue damage parameter for CFRP composites

Bourchak et al. (2007) tested for the correlation between AE energy and fatigue damage of CFRP laminates. This research tested two types of CFRP: one from Augusta-Westland Helicopters and one from Dowty Aerospace Propellers. The specimens were first tested with a continuous load or static test while AE was monitored. The specimen was then tested using a fatigue test while collecting AE. The paper found that AE energy has a good general correlation with stress strain curves and AE energy showed the ability to indicate effective static and fatigue failure states (Bourchak et al. 2007).

Determination of impact behavior of ABS from acoustic emission, ultrasound and optics

Dundar et al. (2015) used AE attributes to study the impact behavior on an Acrylonitrile-butadiene-styrene (ABS) specimen. A mass was dropped from various heights onto the ABS specimen and AE parameters were used to determine the damage level to the specimen. Duration, rise-time, amplitude, and rise-time/duration were all plotted against the impact energy of the test. Each of the parameters peaked at the middle impact energy leading to the conclusion that the greatest amount of damage to the specimen occurred at the middle impact energy rather than the highest. This was confirmed with laser

scanning microscopy. Therefore, parameters that were investigated directly correlated with the damage, but there is a need for more testing with varying levels of impact energy.

2.4 AE and AI

Structural Health Evaluation Using Advanced Acoustic Emission Parameters

Ma et al. (2019) designed an indoor experiment to investigate the relationship between signal parameters and loads. The authors found relationships between AE parameters or multi-parameters with cracks before applying a DNN model that would classify the structural damage. Finally, the authors applied their findings to two on-site bridges and were able to detect certain problem areas.

This experiment consisted of 10 prestressed beams undergoing a cyclic loading four point bending test. There were 5 prestressed C40 beams called group 1 and 5 prestressed C50 beams called group 2. The beams were 200mm wide by 250 mm tall by 1200 mm long.

The monitoring system used in the research is the acoustic emission signal detection instrument SAEU2S, a digital acoustic emission acquisition system produced by Beijing Science and Technology Company, with 60 strain and displacement monitor channels. Four acoustic emission sensors were distributed in the central beam evenly with a distance of 200 mm.

The C40 beams and C50 beams were divided into load steps based on their yield load and ultimate load. Those steps were then divided into sub steps. Step 1 refers to the loading and unloading portions of one tenth of the ultimate capacity load. Step 11 only refers to the loading and step 12 refers to the unloading and this pattern continues.

Analysis was divided into three steps. Step 1 was data preprocessing. Since not all the original parameters of the signals were suited for analysis, it was necessary to change them to other forms or other parameters for analysis. Step 2 was the characteristic analysis of each parameter. This step mainly refers to making useful data out of raw data received from the sensors. Step 3 was the assessment of signal activities. This process gave signal activities a comprehensive classification based on the combination of several parameters.

The first characteristic analysis was converting quantity (Q) to log quantity (LQ). This involved quantifying the number of hits in a load step and then calculating the logarithm of that number to make the numbers more manageable.

The authors found the max amplitude, the average amplitude, and a variable AK, which is the number of hits over 60 dB over the total number of hits for the load step. Ma et al. (2019) concluded that, "High loads correspond to high amplitudes, but low loads may also have high amplitudes for the existence of noise signals. The numbers of signals also have an impact on the average amplitudes, especially when they are very low; 2) Low average amplitudes correspond to small loads; 3) The maximum amplitude generally reaches a high value when the load force is high. Amplitudes more than 90 dB may be a signal for failure".

EA is a parameter where the whole signal energy E is divided by the number of signals in the same stage as E. Several findings are as follows: "1) Three stages can be divided by EA: When EA is 0 ~ 100, there is almost no crack activity; When EA is 100 ~ 200, there is some crack activity, but it is not obvious; When EA is above 200, there is a

huge amount of crack activity; 2) The greater the value of EA, the more dangerous of the structure. 3) EA is affected by structural materials" (Ma et al. 2019).

V_e is taken as the average velocity of signals for a determined amount of time. In this case 10 seconds. Four stages can be divided for the same beam, no cracks, micro-cracks begin, micro-crack growth and macrocrack growth. The highest V_e happens as macro-cracking begins. Then there is a decline after this stage.

RA in the article is defined as the rising time of a signal divided by its peak amplitude. It was concluded that RA is a good parameter to judge whether the strength of structures reaches their designed strength.

LE is a new parameter, calculated by the last time of a signal divided by its energy. "The results show that LE is about 1.1 ~ 1.3 when the strength degree of a specimen meets its design requirement" (Ma et al. 2019). However, when the strength does not reach the design strength, LE will be higher than normal.

Ma et al. (2019) trained a deep neural network to classify the AE hits based on the observations and conclusions drawn from the study of the parameters stated earlier. Firstly, amount and amplitude give the structure a preliminary judgment of whether to continue the calculation. If the signals are too few and the amplitudes of the signals are very low, the DNN recognizes that this means there is no crack activity. Secondly, it observes Amean, RA and LE to give the structure a strength determination. Finally, a final assessment of signal activities is determined by the combination of LQ, Amax, EA, V_e, AK.

If the data survives the first stage it moves onto the second stage where the Amean RA and LE determine its strength. Then, if it conforms to strength, it is given a damage degree ranging from D0-D3 where D3 is a severe damage degree.

The next step was to applied sensors on a new and an old bridge in the field and collect data as vehicles passed. The results were a successful finding of problem areas in the bridges.

Ma et al. (2018 concludes that an experiment had been successfully designed that retrieved AE from beams and used those signals to determine the characteristics of the parameters and their correlations with one another. A DNN was used to analyze these parameters and apply this method to two real world bridges where it was successful in that data collection. There are still limitations, for example AE characteristics are influenced by materials and other strengths so the paper calls for more work in this area to improve precision and accuracy of structural evaluation.

Identification of damage mechanisms in self-reinforced polyethylene composites by using pattern recognition techniques on AE data & Unsupervised pattern recognition of acoustic emission from full scale testing of a wind turbine blade

Yang et al. (2009) tested ten samples of Ultra High Molecular Weight Polyethylene Fiber Reinforced Low Density Polyethylene Composites (UHMWPE/LDPE). The AE system monitored 200 mm by 20 mm specimens continuously during a monotonic tensile test. The experiment utilized two WD sensors with a resonance range of 100-1000 kHz with a distance of 60 mm between them. Data preprocessing was carried out by a software called Noesis Professional V4.0. The authors then used an Unsupervised Pattern Recognition (UPR) technique to cluster the data into different damage classes. Only 9 features were used for this process. The UPR was able to identify four different damage

modes. Once identified the labeling and signal classes were then used as inputs for the Supervised Pattern Recognition (SPR) system to identify the rest of the unknown AE signals. The conclusion is that it was successful in the recognition of several different AE signals that were also confirmed by the Scanning Electron Microscope (SEM). Yang et al. (2009) also states that "[because] the SPR system is mathematically reliable it can be used for any other unknown data set of UHMWPE/LDPE composites".

Another UPR technique using Noesis was utilized in Kouroussis et al. (2000) for the classification of AE signals collected from the static and fatigue loading of a wind turbine blade. After the UPR clustering was performed a back propagation neural network (BPNN) was trained to classify the AE hits into one of seven damage classes.

Source localization on large-scale canisters for used nuclear fuel storage using optimal number of acoustic emission sensors

Ai et al. (2021) tested the detection of impact on aircraft using different machine learning techniques. A steel ball was dropped 60 times on 60 different locations of an aircraft elevator component and AE data was collected for each drop. 15 features were used and inputted into a random forest machine learning technique. The study was able to identify the importance of features in the accuracy of the model. In the paper 3 different machine learning techniques were compared: Sparse Autoencoder (SAE), Random Forest, and ANN. Accuracy was measured by the source location categorization of the hit. The model was responsible for classifying the AE data into 1 of 3 zone locations. The most accurate was the SAE, however, the Random Forest was within 2 percentage points and required 0.2 seconds of computing time while the SAE required 681.4 seconds of

computing time. The authors determined that for the source location of impact on an aircraft component the random forest machine learning technique was the optimized solution taking in account the computing time and accuracy. The ANN was the least accurate but required little to no computing time as well.

Neural network detection of grinding burn from acoustic emission

Wang et al. (2001) designed an experiment in which an AE sensor was attached to a specimen that was cut with a Norton Grinder. The experiment attempted to classify the AE signals into "burn' and "non-burn" categories. The authors attempted to classify the data by using a statistical analysis method on individual features collected during the test. They also used a neural network to identify and classify the data. The paper concluded that while there were certain statistical differences in single attributes it was found to have a very limited capability to predict the grinding state while the neural network was essentially perfect.

Acoustic emission signal analysis and artificial intelligence techniques in machine condition monitoring and fault diagnosis: A review

Hassan et al. (2014) reviewed the literature surrounding 4 different AI methods for the classification of AE data including ANN, fuzzy logic, genetic algorithms, and support vector machines. The authors concluded that ANN was the most popular method as well as one of the most successful for the classification of AE data for condition monitoring.

2.5 Figures

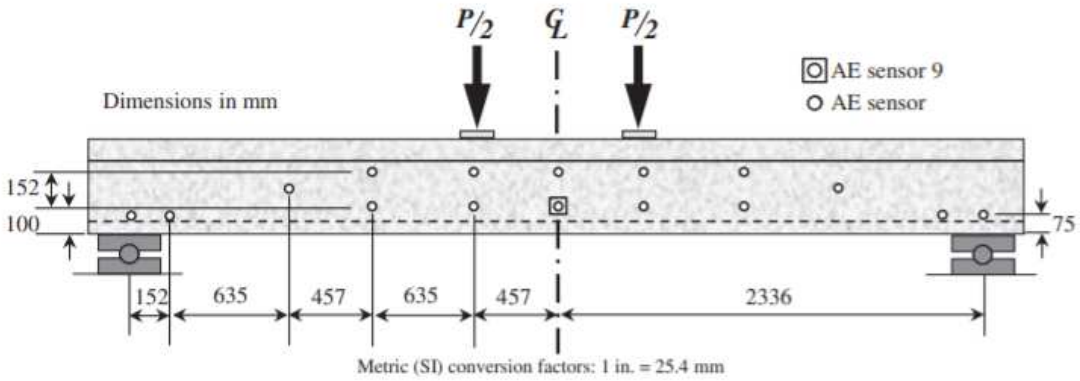

Figure 2.1 Experimental setup for Elbatanouny et al. (2014)

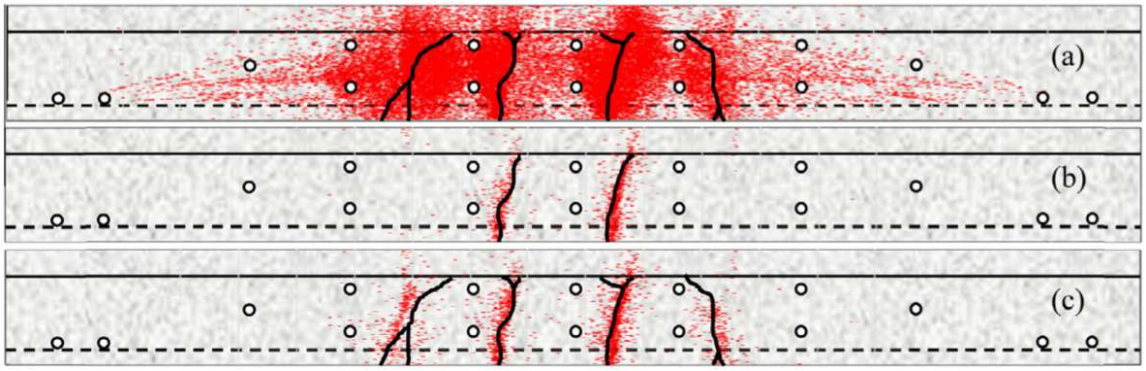

Figure 2.2 Source location from Elbatanouny et al. (2014)

2.6 References

Aggelis, D. G., Verbruggen, S., Tsangouri, E., Tysmans, T., & van Hemelrijck, D. (2013). Characterization of mechanical performance of concrete beams with external reinforcement by acoustic emission and digital image correlation. *Construction and Building Materials*, *47*. https://doi.org/10.1016/j.conbuildmat.2013.06.005

Ai, L., Soltangharaei, V., Bayat, M., van Tooren, M., & Ziehl, P. (2021). Detection of impact on aircraft composite structure using machine learning techniques. *Measurement Science and Technology*, *32*(8). https://doi.org/10.1088/1361-6501/abe790

Alwosheel, A., van Cranenburgh, S., & Chorus, C. G. (2018). Is your dataset big enough? Sample size requirements when using artificial neural networks for discrete choice analysis. *Journal of Choice Modelling*, *28*. https://doi.org/10.1016/j.jocm.2018.07.002

ASTM. (2017). ASTM D6272 Standard Test Method for Flexural Properties of Unreinforced and Reinforced Plastics and Electrical Insulating Materials by Four-Point Bending. *Annual Book of ASTM Standards*, *02*(Reapproved).

Bourchak, M., Farrow, I. R., Bond, I. P., Rowland, C. W., & Menan, F. (2007). Acoustic emission energy as a fatigue damage parameter for CFRP composites. *International Journal of Fatigue*, *29*(3). https://doi.org/10.1016/j.ijfatigue.2006.05.009

Dundar, M. A., Ayorinde, E., & Al-Zubi, M. (2015). Determination of impact behavior of ABS from acoustic emission, ultrasound and optics. *ASME International Mechanical Engineering Congress and Exposition, Proceedings (IMECE)*, *9–2015*. https://doi.org/10.1115/IMECE2015-52948

Elbatanouny, M. K., Ziehl, P. H., Larosche, A., Mangual, J., Matta, F., & Nanni, A. (2014). Acoustic emission monitoring for assessment of prestressed concrete beams. *Construction and Building Materials*, *58*. https://doi.org/10.1016/j.conbuildmat.2014.01.100

Hassan Ali, Y., Abd Rahman, R., & Raja Hamzah, R. I. (2014). Acoustic emission signal analysis and artificial intelligence techniques in machine condition monitoring and fault diagnosis: A review. *Jurnal Teknologi (Sciences and Engineering)*, *69*(2). https://doi.org/10.11113/jt.v69.3121

Kavzoglu, T. (2009). Increasing the accuracy of neural network classification using refined training data. *Environmental Modelling and Software*, *24*(7). https://doi.org/10.1016/j.envsoft.2008.11.012

Kouroussis, D., Anastassopoulos, A., & Vionis, P. (2000). Unsupervised pattern recognition of acoustic emission from full scale testing of a wind turbine blade. *Journal of Acoustic*.

Ma, G., & Du, Q. (2020). Structural health evaluation of the prestressed concrete using advanced acoustic emission (AE) parameters. *Construction and Building Materials*, *250*. https://doi.org/10.1016/j.conbuildmat.2020.118860

Pollock, A. A. (1973). Acoustic emission - 2. Acoustic emission amplitudes. *Non-Destructive Testing*, *6*(5). https://doi.org/10.1016/0029-1021(73)90074-1

Prem, P. R., Murthy, A. R., & Verma, M. (2018). Theoretical modelling and acoustic emission monitoring of RC beams strengthened with UHPC. *Construction and Building Materials*, *158*. https://doi.org/10.1016/j.conbuildmat.2017.10.063

Radiuk, P. M. (2018). Impact of Training Set Batch Size on the Performance of Convolutional Neural Networks for Diverse Datasets. *Information Technology and Management Science*, *20*(1). https://doi.org/10.1515/itms-2017-0003

Saxena, A., & Saad, A. (2006). Genetic algorithms for artificial neural net-based condition monitoring system design for rotating mechanical systems. *Advances in Soft Computing*, *34*. https://doi.org/10.1007/3-540-31662-0_11

Stone, D. E. W., & Dingwall, P. F. (1977). Acoustic emission parameters and their interpretation. *NDT International*, *10*(2). https://doi.org/10.1016/0308-9126(77)90079-7

Tong, F., & Liu, X. (2005). Samples selection for artificial neural network training in preliminary structural design. *Tsinghua Science and Technology*, *10*(2). https://doi.org/10.1016/S1007-0214(05)70060-2

Wang, Z., Willett, P., Deaguiar, P. R., & Webster, J. (2001). Neural network detection of grinding burn from acoustic emission. *International Journal of Machine Tools and Manufacture*, *41*(2). https://doi.org/10.1016/S0890-6955(00)00057-2

Yang, B. L., & Yan, X. (2009). Identification of damage mechanisms in self-reinforced polyethylene composites by using pattern recognition techniques on AE data. *Nondestructive Testing and Evaluation*, *24*(3). https://doi.org/10.1080/10589750802195477

Yang, S., & Browne, A. (2004). Neural network ensembles: combining multiple models for enhanced performance using a multistage approach. *Expert Systems*, *21*(5). https://doi.org/10.1111/j.1468-0394.2004.00285.x

CHAPTER 3

METHODOLOGY

The goals of this project are a) to analyze acoustic emission waveforms associated with representative truck axle loads; and b) to correlate the waveforms to the loading of the structure. This chapter addresses the testing setup and forms of analysis.

3.1 Flat slab test setup

Flexural tests were conducted on slab specimens that were provided by the SCDOT. The slabs were originally used as a portion of a bridge, likely for at least 30 years, and were then stored in an SCDOT facility. The slabs used were 15 feet long. The 15-foot slabs were 8.25 inches thick and 5.5 feet wide. Based on SCDOT drawings, typical reinforcement for precast reinforced concrete flat slabs is No. 7 bars @ 6 in. on center longitudinally and No. 4 @ 12 in. on center transversely (Figure 3.1). Based on the age of the slabs, it was assumed that the compressive strength of concrete was $f_c' = 4000\ psi$ and the *yield strength of steel* was $f_y = 40000\ psi$. This thesis will focus on 2 different tests of unstrenghtened 15-foot slabs. Figure 3.2 shows the test setup for a typical slab.

3.2 Testing

Two 15-foot precast reinforced concrete flat slabs were tested. The test numbering scheme along with a brief description of the slab are presented in Table 3.1.

The symbols used in the table are defined as follows: L is the length of slab, E is the width of slab, D is the depth of slab, W is the width of bearing, a is the length of bearing

pad, b is the width of bearing pad, c is the distance from center to center from one bearing pad to the other, d is the width of the spreader beam, F is the length of spreader beam, and X is the shear span length (distance of loading point from the supports).

Each of the slabs underwent laboratory flexural tests. The loading of the slabs was step-wise cyclic, meaning the slab was initially loaded to 2 kips then the load was increased to 10 kips (referred to as load step 1); and then it was unloaded back to 2 kips and increased to 20 kips; (referred to as load step 2). The test continued this way for 6 load steps (60 kips). The load versus time data for each of the tests included in this thesis are presented in Chapter 4. This thesis will focus on load step 1 through load step 3 because that is the anticipated range of vehicle loads that these flat slab superstructures may support throughout their lifetimes. More specifically, this thesis looks to find the difference in acoustic emission data between load step 2 and load step 3. Figure 3.2 shows a schematic of the typical test set up while Figures 3.3 and 3.4 present photos of the test set ups.

3.3 AE Data Collection

Acoustic emission data was collected using the Sensor Highway II data acquisition system and 4 broadband sensors (type WDI). The system was manufactured by Mistras Group, Inc. of Princeton Junction, New Jersey. Broadband sensors were selected because they have a wide range of operating frequencies; in other words, the broadband sensors can capture more frequency components than resonant AE sensors. The sensors were placed at L/3 and W/3locations. Sensor locations can be seen in Figure 3.5.

Data was continuously taken as the tests progressed with a threshold of 50 decibels. The threshold was determined to prevent extraneous data from being picked up by the

sensors. The Sensor Highway II was able to collect large amounts of data from each test and extract 13 features from each waveform collected. Table 3.2 lists the 13 features as well as their definitions. The number of data points collected for T1 are presented in Chapter 4.

3.4 Single Attribute Analysis Procedure

The first attempt at classification analysis was extracting single attribute data from one test and determining whether the attribute was a reliable indicator for classification within that test data. Three attributes were chosen based on prior knowledge of AE behavior and some preliminary results. The three features that were analyzed were amplitude, rise time, and energy. It was hypothesized that these three attributes would differ the most between load steps 1 to 3 within the same test. A basic statistical analysis was conducted for each of the three features and probability density functions were determined for each feature collected during each load step. More on this can be found in Chapter 4.

3.5 ANN Procedure

Moving forward T1 will refer to test 1 and T2 will refer to test 2. L2 will refer to load step 2 or 20 kips while L3 will refer to load step 3 or 30 kips. For example, the abbreviation T1L2 refers to the data collected during test 1 and load step 2.

Due to the large number of data points collected and the large number of attributes of AE waveforms an artificial neural network was developed to classify the hits into two groups, L2 and L3. The neural network goes through three steps to come up with its classification: training, validation, and then testing. At first, data from T1, which included all the hits from T1L2 and T1L3 (about 24,000 hits) was fed into the neural network, and

it randomly selected one third of the data for training, another third for validation and the last third for testing. This caused an imbalance issue because most of the hits in the overall data set belonged to T1L3. So, the network became very good at classifying T1L3 but was inaccurate at classifying T1L2. More of this issue along with the results, can be found in Chapter 4. Figure 3.6 shows the imbalanced process of the neural network. To combat the imbalance issue, a new code was developed that would train, validate, and test on an equal number of datapoints from each load step. It was determined that the number of datapoints belonging to T1L3 was about 10 times that of T1L2. So, to even out the data 10 different models were trained and validated with all the data points from T1L2 and a random tenth of the data from T1L3. These models were then tested on data that was taken before training or validation and each model cast a classification vote. The majority rule applied to the models' votes and a final classification was determined thus creating an ANN ensemble. The product of combining neural networks to improve accuracy is called an ANN ensemble. Figure 3.7 shows the process of neural network ensemble. This process will be referred to as balanced training.

Once the algorithm was established the optimal number of hidden layers and hidden layer size was determined through iterations of running the code. Optimal number and size were determined based on output accuracy. A chart of the accuracy is shown in Chapter 4. Once optimized, this model was named MT1 for model with T1 training.

After the algorithm was optimized, the trained neural network's reliability was tested using data from an entirely different slab test. For example, the neural network was trained using the data collected from T1, and then the performance of the network was determined by the accuracy of classification of the data collected from T2. MT1's

classification ability was tested using 3 different datasets which were: the data collected during test 2 load step 2 (T2L2), the data collected during test 2 load step 3 (T2L3), and all of the data collected from test 2 (T2). The performance of the model was determined by the output accuracy. A flowchart of this process can be seen in Figure 3.9.

3.6 Tables

Table 3.1 Slab characteristics and geometry

Test	*Location of Test*	*Source of slabs*	*Date*	*L (ft)*	*E (ft)*	*D (in)*	*W (in)*	*a (in)*	*b (in)*	*c (in)*	*d (in)*	*F (in)*	*X* (ft)*
T1	UofSC	Callhoun Falls bridge	8/20/21	15	5.5	8.25	9.5	8.5	8.5	40	8.5	51.7	5.43
T2	UofSC	Callhoun Falls bridge	7/22/21	15	5.5	8.25	9.5	8.5	8.5	40	8.5	51.7	5.43

Table 3.2 AE feature and definitions.

No	***Features***	***Descriptions***
1	Amplitude (dB)	The maximum amplitude at the peak
2	Count	The number of threshold crossings
3	Rise time (μs)	Time interval between first threshold crossing and maximum amplitude
4	Duration (μs)	Time between first and last threshold crossing of signal
5	Average frequency (kHz)	Counts/Duration
6	Root mean square (RMS) (V)	The effective voltage with a characteristic time T_{RMS} for average ranging from 10 to 1000 ms
7	Average signal level (ASL) (V)	The effective voltage with a characteristic time T_{ASL} for average ranging from 10 to 1000 ms

8	Energy	The measure of the electrical energy measured for an AE signal
9	Absolute energy	The absolute measure of the electrical energy measured for an AE signal
10	Reverberation frequency (kHz)	Frequency after the peak
11	Initial frequency (kHz)	Frequency before the peak
12	Signal strength	A parameter to evaluate the AE source strength
13	Counts to peak (PCNTS)	The number of threshold crossings from the first threshold crossing to the peak

3.7 Figures

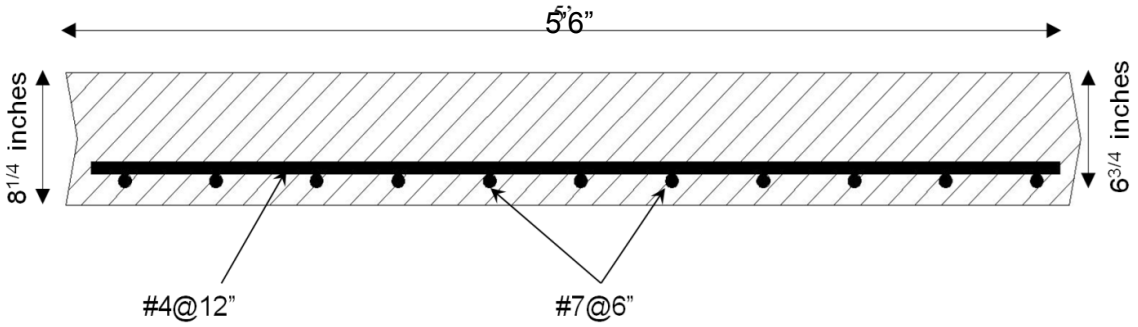

Figure 3.1 Reinforcement of the typical flat slab

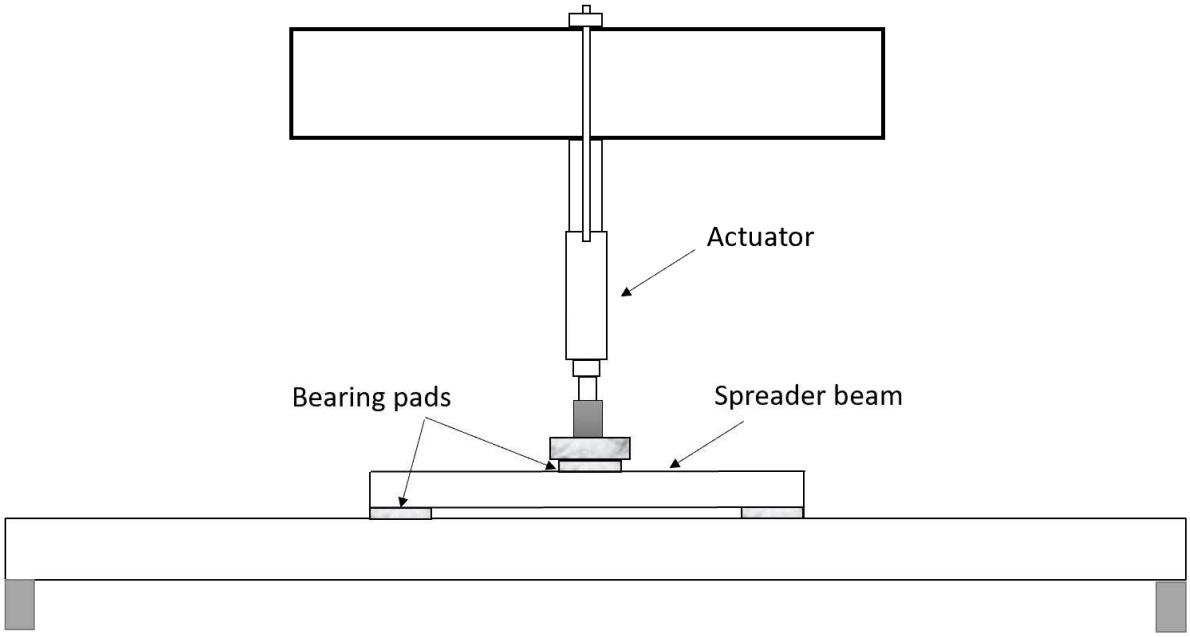

Figure 3.2 Scheme of flexural test set up

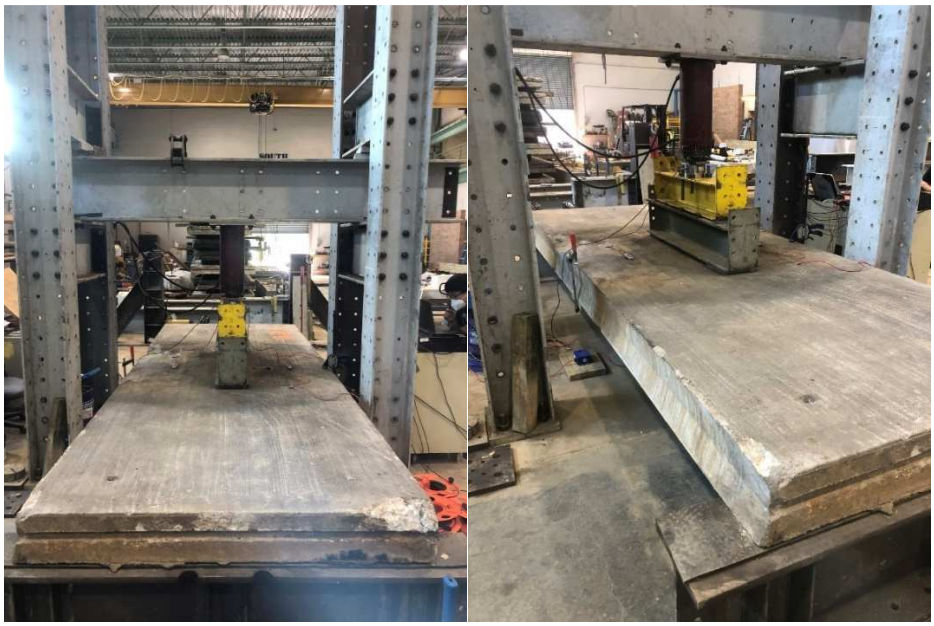

Figure 3.3 Photos of T1 test setup

Figure 3.4 Photos of T2 test setup

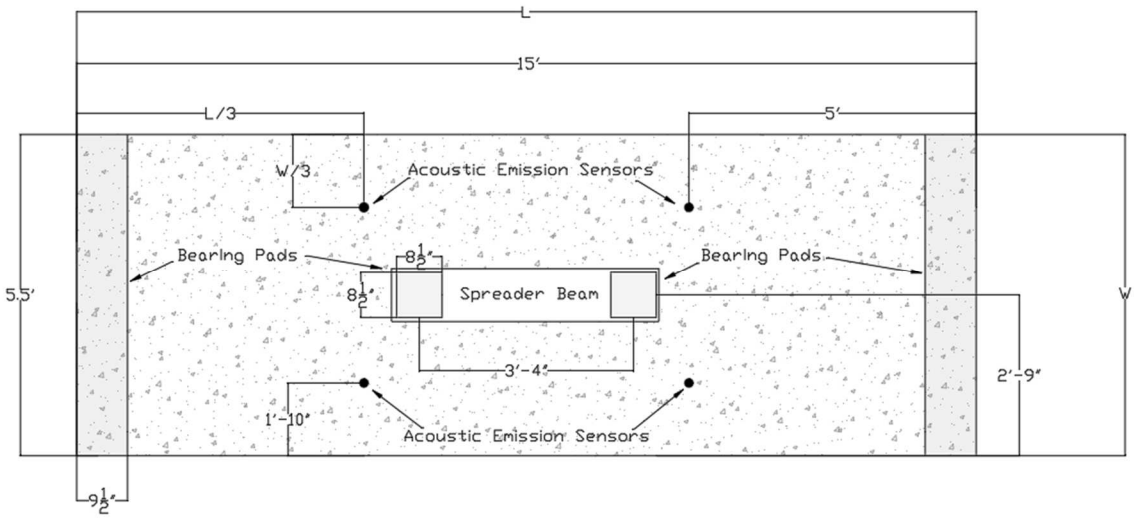

Figure 3.5 A scheme of the test setup and AE sensor locations

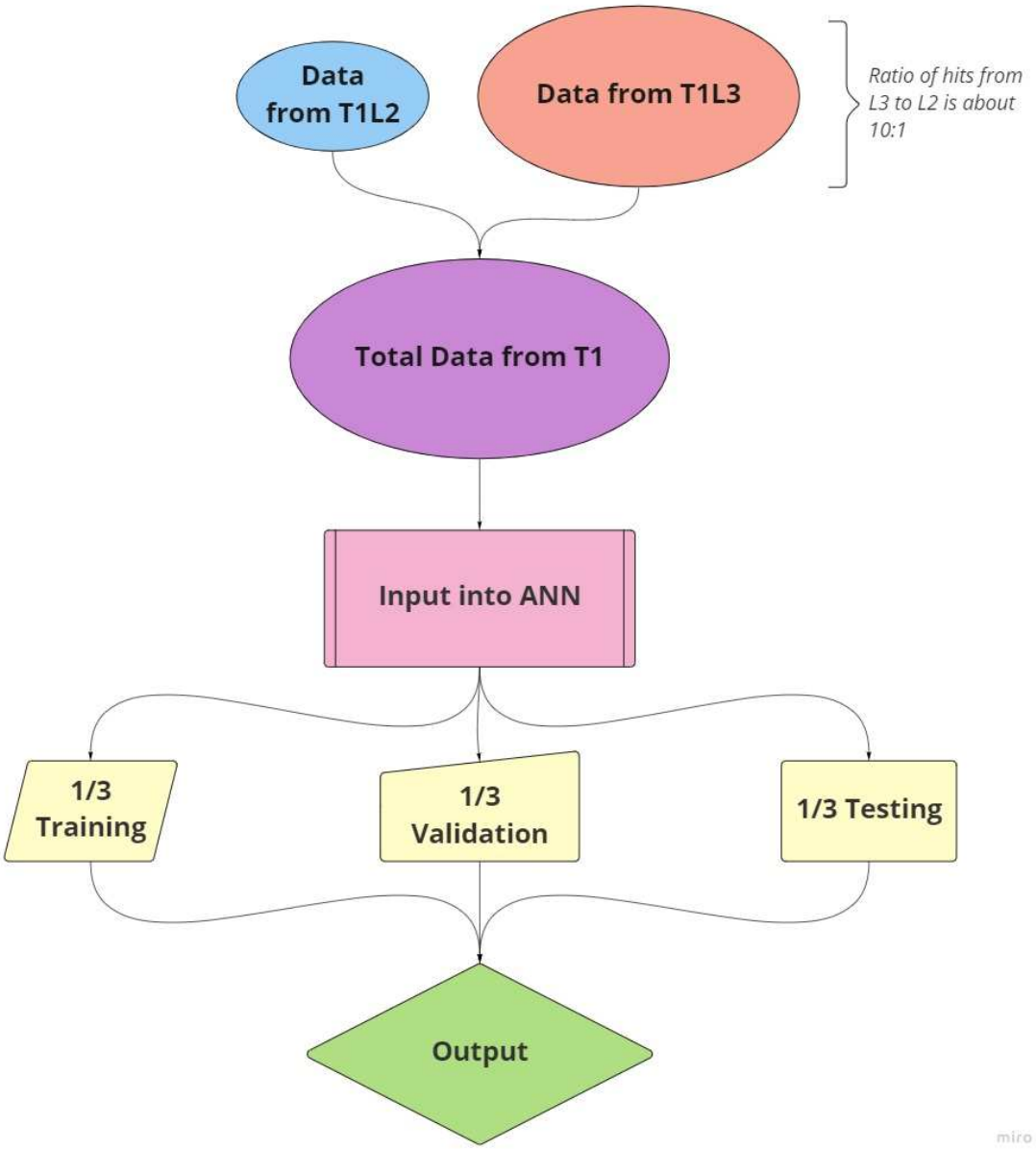

Figure 3.6 Initial flowchart for the ANN

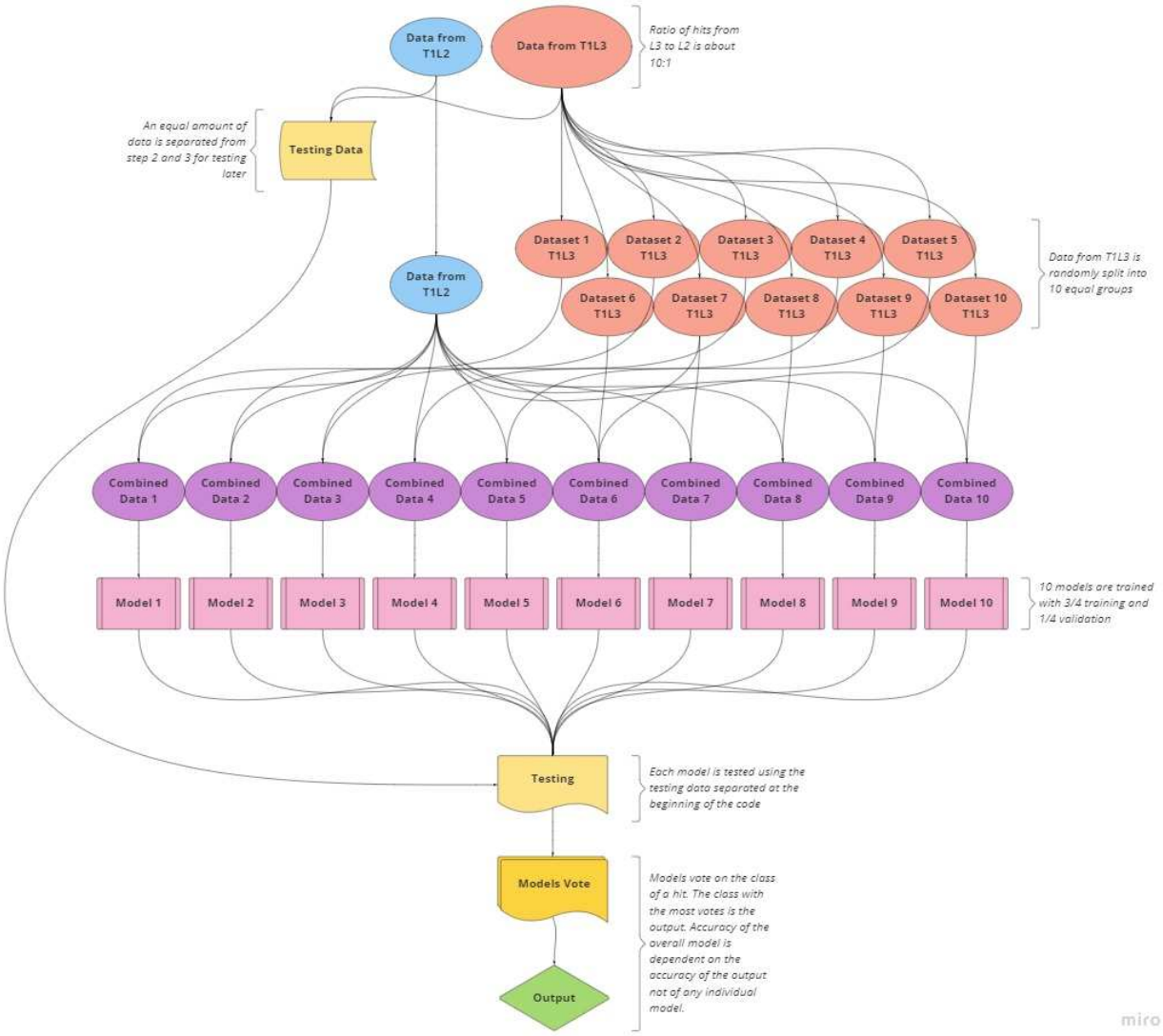

Figure 3.7 Balanced flowchart for the ANN

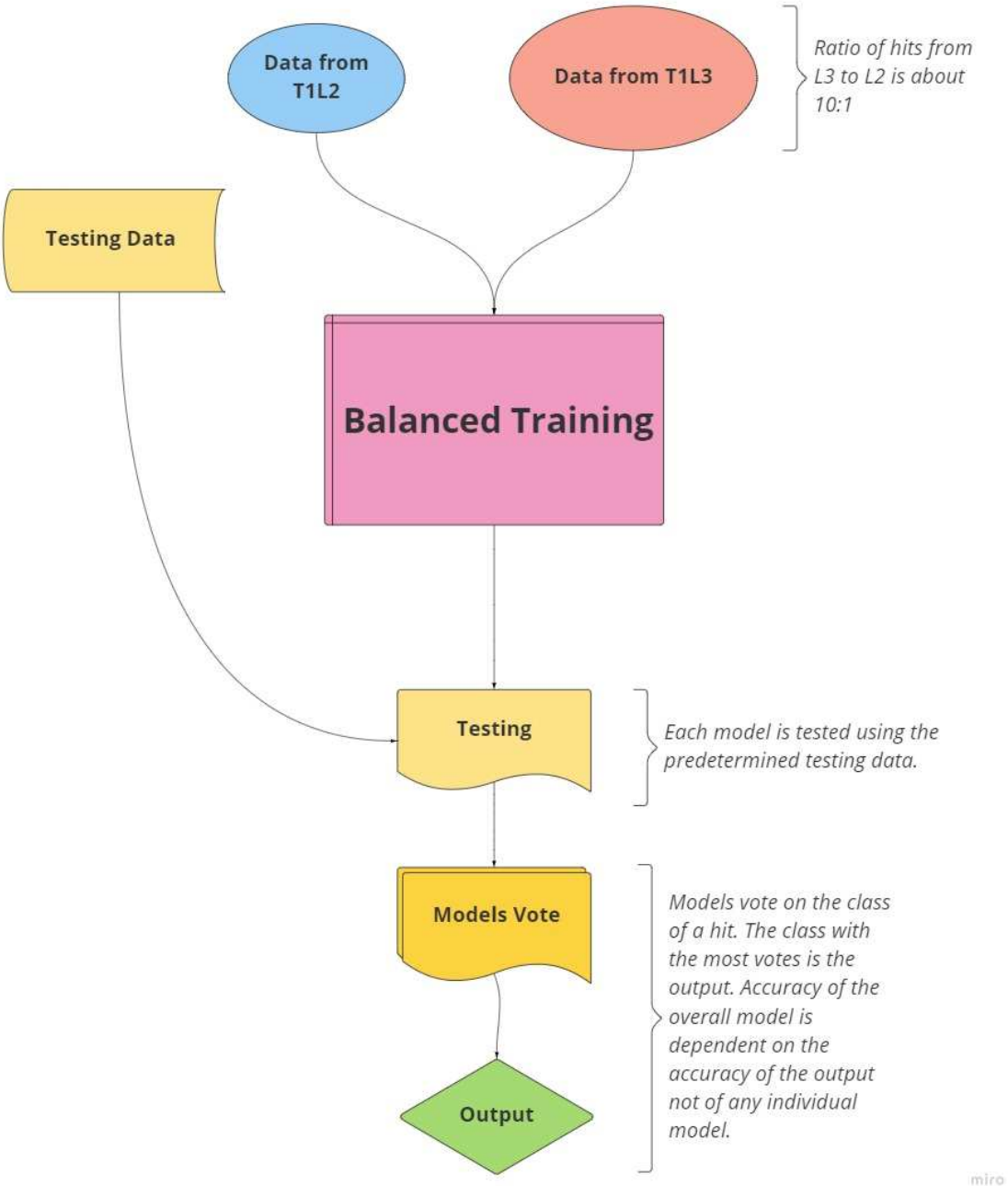

Figure 3.8 Flowchart of MT1 tests

CHAPTER 4

FINDINGS & DISCUSSION

In this chapter the physical results of the flexural tests are presented in 4.1. The results of the statistical analysis of amplitude, rise-time, and energy are presented in 4.2. Lastly, the results of 6 tests on 3 different ANN models are presented in 4.3.

4.1 Flexure Test Results

In this section the results of the ultimate moment testing are presented. The load versus time charts for each test presented in Figures 4.1 and 4.2, showing minor differences between the loading of the tests. The most obvious difference is the inconsistency of the load during the load hold period of the test. The reason behind this inconsistency is that the Enerpac hydraulic pump, that is used to apply load, becomes more sensitive as the pressure of the system increases. While a slight variation of the operator's movement at lower pressures is insignificant, a slight variation at higher loads will cause the spikes seen in the charts. Another difference is shown in T2 when it is initially loaded to the first step, instead of 2 kips. Another noticeable difference is the duration of T2 as its hold periods are longer than that of T1, resulting in a duration of about 500 seconds versus 400 seconds for T1

Because the slabs were tested to failure, the ultimate moment capacity is compared. It is important to mention the mechanical properties because AE data may differ based on the mechanical properties of the material. Table 4.1 shows the physical results of each of the tests.

Load versus displacement charts for the failure tests of T1 and T2 can be seen in Figures 4.3 and 4.4 with the 30 kip focus area shown. The load versus displacement charts of L2 and L3 can be seen in Figures 4.5 and 4.6. Lastly the amplitude of the AE data collected for L2 and L3 was overlayed with the load versus displacement curves of each test. These plots can be seen in figures 4.7 and 4.8.

The ultimate moment capacity of the slab was captured when the concrete crushes, therefore the ultimate moment capacity at crushing for T1 was 253 kip-ft and the ultimate moment capacity at crushing for T2 was 256 kip-ft. The midspan displacement at concrete crushing for T1 and T2 was 6.1 in and 7.7 in respectively. The corresponding load at which concrete crushing occurred was 87.5 kips and 88.5 kips for T1 and T2 respectively.

Photos of the failures of the slabs are presented in figures 4.9 and 4.10.

4.2 Single Attribute Analysis Results

The single attribute analysis includes a statistical analysis of the amplitude, rise time, and energy of the hits collected between L1 to L3. All data was compared within one test, T1.

4.2.1 Amplitude analysis

Amplitude was the first attribute analyzed. First, the amplitude of AE hits was plotted along with the loading of the test. This allowed for some visual analysis of the characteristics of the AE feature versus the load step. These plots are presented in figures 4.11 through 4.14. It was determined that L1 would be insignificant from this point moving forward because of the lack of consequential data collected during this step. Attention was then turned to the differences between L2 and L3. These two plots look rather similar, however the differences appear to be that L3 has a greater density of AE hits and a higher peak amplitude. To find more specific differences, simple statistics were extracted for L2 and L3. This data can be seen in Table 4.2 where the upper and lower limits were determined from the following equations

$$Upper\ Limit = \mu + 3 * \sigma \tag{4.a}$$

$$Lower\ Limit = \mu - 3 * \sigma \tag{4.b}$$

where μ is the mean of the sample and σ is the standard deviation.

The average amplitude of L2 was 56.4 dB and L3 was 57.3 dB. The standard deviation for L2 and L3 was 6.31 dB and 6.93 dB, respectively. The upper and lower limits for L2 were 75.3 dB and 37.4 dB while the limits for L3 were 78.1 dB and 36.5 dB. The maximum amplitude achieved for L2 was 88 dB while L3 reached a max amplitude of 99 dB. The number of hits collected during L2 was 2263 and for L3 it was 20981.

A frequency chart was created for L2 and L3. This can be found in Figures 4.15 and 4.16. This was the first time that the parts of the load steps were also compared by breaking the steps into loading and unloading periods. This chart shows that there were

little to no additional hits collected during the unloading phase for L2, however there is a more significant presence of unloading hits collected for L3.

From the frequency charts, a probability chart was created by taking the number of hits of that amplitude and dividing it by the total number of hits in that load step to get a probability of that amplitude occurring within that load step.

$$P_{A(L2)}(50) = \frac{\#\ of\ 50\ amplitude\ hits\ in\ L2}{total\ \#\ of\ hits\ in\ L2} \quad (4.c)$$

This chart can be seen in figure 4.17. The curves are very similar, and classification of hits solely from the amplitude feature may be problematic, so a similar analysis was done on the rise-time parameter for the load steps.

4.2.2 Rise time analysis

After comparing the amplitude, the rise time was statistically analyzed. The average rise time of L2 was 82.3 μs and L3 was 123 μs. The standard deviation for L2 and L3 was 89.1 μs and 154 μs respectively. The upper and lower limits for L2 were 350 μs and 1 μs while the limits for L3 were 586 μs and 1 μs. The max rise time achieved for L2 was 661 μs while L3 reached a max rise time of 1430 μs. The number of hits collected during L2 and L3 remained the same.

The differences in the basic statistics were more apparent than the amplitude parameter so the probability of each rise time was plotted according to the same equation used above. This plot can be seen in Figure 4.18. A probability density function for L2 and L3 was also estimated using the exponential formula below:

$$\lambda e^{-\lambda x} \quad (4.d)$$

Where λ is a rate parameter dependent upon mean and *e* is Euler's number. These functions were then compared and the comparisons can be seen in Figure 4.19.

4.2.3 Energy analysis

Lastly, energy was statistically analyzed. The average energy of L2 was 12.2 and L3 was 21.9. The standard deviation for L2 and L3 was 20.8 and 56.5 respectively. The upper and lower limits for L2 were 74.5 and 0 while the limits for L3 were 191 and 0. The max energy achieved for L2 was 349 while L3 reached a max energy of 1920. The number of hits collected during L2 and L3 remained the same.

The differences in the basic statistics were less apparent than rise time but more apparent than the amplitude parameter, so the probability of the energy was plotted according to the same equation used above. This plot can be seen in Figure 4.20. A probability density function for L2 and L3 was also estimated using the exponential formula above. These functions were then compared and the comparisons can be seen in Figure 4.20.

4.2.4 Summary and Discussion

In this section a statistical analysis of 3 AE features is presented. The goal of this analysis was to a) quantify the differences between the features collected during different load steps and b) determine whether the differences can be exploited to classify the data. It was concluded that, while there are some significant statistical differences, classifications are difficult to extract from a single attribute analysis. This conclusion is what led to the

construction of an ANN that allowed analysis of all 13 attributes for classification into load steps.

4.3 ANN Results

4.3.1 Introduction

An artificial neural network was developed to classify the AE hits using all 13 extracted features from the Sensor Highway II system. The goal of the algorithm was to accurately classify AE hits into load steps. In this section the results of 3 tests on a balanced ANN ensemble are presented. The model mentioned in Chapter 3 and called MT1 was tested on the classification of test 2 load step 2 data (T2L2), test 2 load step 3 data (T2L3), and test 2 data (T2). The performance of the model was measured by its accuracy which was calculated by taking the number of correctly classified hits over the total number of hits for that test.

4.3.2 Imbalanced Neural Network Results

The first neural network developed took data from T1 which included all of the hits from L2 and L3 (over 23,000 hits) and fed it into the neural network and then randomly selected one third of the data for training, another third for validation, and the last third for testing. The confusion matrix of that test is shown in Figure 4.22.

This model had a 27.2% recall rate in the classification of L2, a 97.9% recall rate in the classification of L3, and an overall accuracy of 90.8%. The model is extremely accurate at classifying L3 however it is inaccurate at the classification of L2. This issue was determined to occur because the model was taking a random third of the data set for training, validation, and testing. The problem with this method is that the number of hits in

the data set belonging to L3 outnumber the hits belonging to L2 by a ratio of 10:1. So the data that the model was trained with a majority of L3 data points and very few L2 data points. This caused the model to be very accurate at classifying L3 but very poor at classifying L2.

4.3.3 Balanced Neural Network Results

To address this issue a balanced training and testing data set was developed where 10 different models were trained using even data from both L2 and L3. Moreover, the models were tested, each model voted, and the classification of the load step was determined by the majority of the models. This model had a 90.5% recall rate in the classification of L2, an 81.2% recall rate in the classification of L3, and an overall accuracy of 86.0%. While the overall accuracy of the model may have dropped by 4.8% the recall rate of L2 was increased by 65.3% which means this model is much better suited at classifying both L2 and L3 data hits. The confusion matrix for this model can be seen in Figure 4.23.

This model was then further optimized by determining the ideal number of neurons and hidden layers. The model was run 10 times for every neuron size from 20 to 30, and an average overall accuracy was determined. An average must be taken because the selection of data is random which leads to a slight variability in performance from test to test. From this an optimal neuron number was found. The same process was repeated for the hidden layer size. The optimal number of neurons was found to be 23 and the ideal hidden layer size was determined to be 1 with the overall accuracy of the model being 85.65%. Charts showing these accuracies can be found in Table 4.5 and Table 4.6.

4.3.4 MT1 Neural Network Results

Once optimized this model was named MT1 and then tested against different tests to observe its reliability against data that it had never seen before. The model was tested on all the data points from T2 and then tested on T2L2 and T2L3 separately. The rationale behind separate testing was to provide data from L2 or L3, but not both, since the model needs to be able to classify the data collected for an individual load step. If the majority of the classification belongs to one load step, then the model can identify that vehicle as belonging to L2 or L3.

It was observed that the model trained solely on the T1 data set was still accurate in the classification of the data points from T2. The model was 87.2% accurate in the classification of only T2L2 and 70.7% accurate in the classification of only T2L3. The model also had an overall accuracy of 73.0% against all the data from T2. The confusion matrices for the tests on this model can be seen in Figures 4.24 through 4.26.

4.4 Tables

Table 4.1 Mechanical test results from T1 & T2

	T1	T2
TOTAL MOMENT AT CONCRETE CRUSHING (KIP-FT)	253	256
DISPLACEMENT AT CONCRETE CRUSHING (IN)	6.1	7.1
LOAD AT CONCRETE CRUSHING (KIPS)	87.6	88.6
YIELD MOMENT (KIP-FT)	219	213
YIELD DISPLACEMENT (IN)	1.17	1.04
YIELD LOAD (KIPS)	75.0	72.8
MAX TOTAL MOMENT (KIP-FT)	254	256
MAX DISPLACEMENT (IN)	6.54	7.71
MAX LOAD (KIPS)	87.9	88.6

Table 4.2 Amplitude statistics for T1

AMPLITUDE (DB)	T1L2	T1L3
MEAN	56.4	57.3
STANDARD DEV	6.31	6.93
UPPER LIMIT	75.3	78.1
LOWER LIMIT	37.4	36.5
UPPER RANGE	88	99
LOWER RANGE	50	50
LOAD STEP HITS	2263	20981

Table 4.3 Rise time statistics for T1

RISE TIME (μS)	T1L2	T1L3
MEAN	82.3	123
STANDARD DEV	89.1	154
UPPER LIMIT	350	586
LOWER LIMIT	0	0
UPPER RANGE	661	1430
LOWER RANGE	1	1
LOAD STEP HITS	2263	20981

Table 4.4 Energy statistics for T1

ENERGY	T1L2	T1L3
MEAN	12.2	21.9
STANDARD DEV	20.8	56.5
UPPER LIMIT	74.5	191
LOWER LIMIT	0	0
UPPER RANGE	349	1920
LOWER RANGE	0	0
LOAD STEP HITS	2263	20981

Table 4.5 Optimization of neuron number

NUMBER OF NEURONS	ACCURACY %										AVERAGE
20	84.6	86.3	84.2	86.4	86.8	84.4	85.8	84.6	83.8	86.2	85.31
21	83	84.7	82.6	83.4	85	84.2	85.1	87.9	83.5	85.1	84.45
22	84.2	84.8	85.1	84.4	87.8	85	84.4	85.7	84.9	85.2	85.15
23	84.9	86.2	85.7	85.1	87.2	87.6	83.2	84.4	85.9	86.3	85.65
24	86.7	85.2	85.6	84.4	84.6	84.8	83.8	86.6	83.2	85.7	85.06
25	85.4	85	84	86.5	86	85.6	87.1	86.6	85.5	85.1	85.68
26	84.7	86.5	84.4	83.8	84.6	84	85.6	84.7	84	84	84.63
27	84.3	86	86	87.4	85.8	85.6	85.1	84	85.5	84	85.37
28	85.2	84.4	85.7	86.3	87.1	84.1	86.7	85.5	84.7	84.2	85.39
29	87.1	85.7	83	85.1	84.6	86.4	86.3	83.5	84.9	87	85.36
30	87.1	84.4	83.5	84.9	85.4	83.5	85.2	84.6	84.9	86.3	84.98

Table 4.6 Optimization of number of hidden layers

HIDDEN LAYERS	ACCURACY %										AVERAGE
1	84.9	86.2	85.7	85.1	87.2	87.6	83.2	84.4	85.9	86.3	85.65
2	84.3	84.6	85	84.8	86.2	85.7	86.8	85.8	84.9	86.4	85.45
3	84.1	87	85.5	86.5	85.1	84.7	83.9	87.5	84.2	83	85.15

4.5 Figures

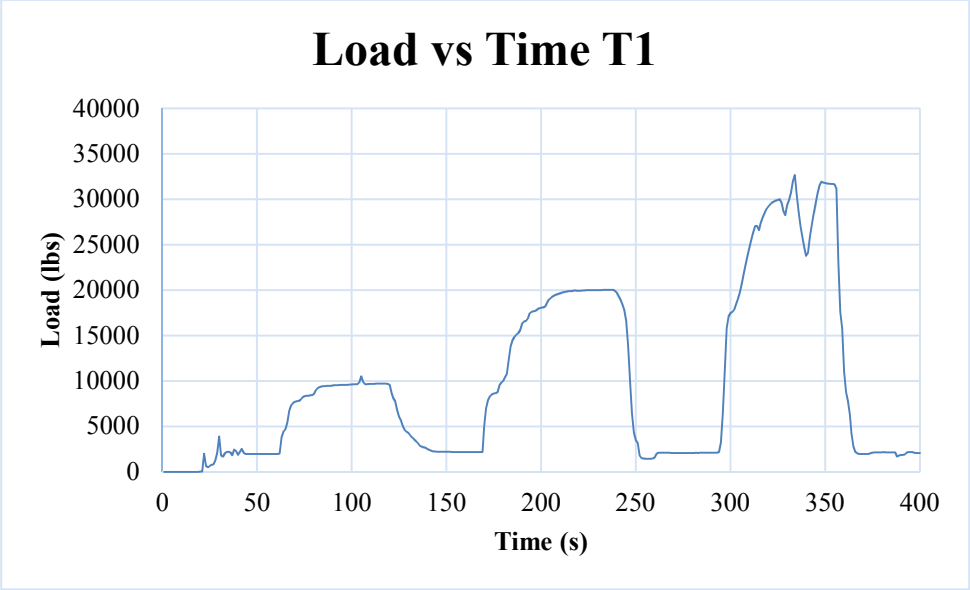

Figure 4.1 Load vs time of T1

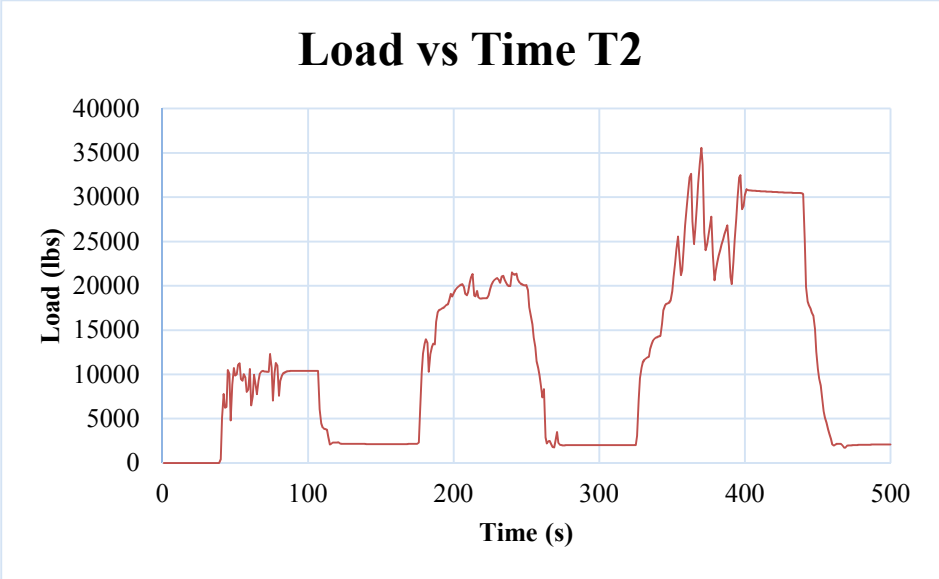

Figure 4.2 Load vs time of T2

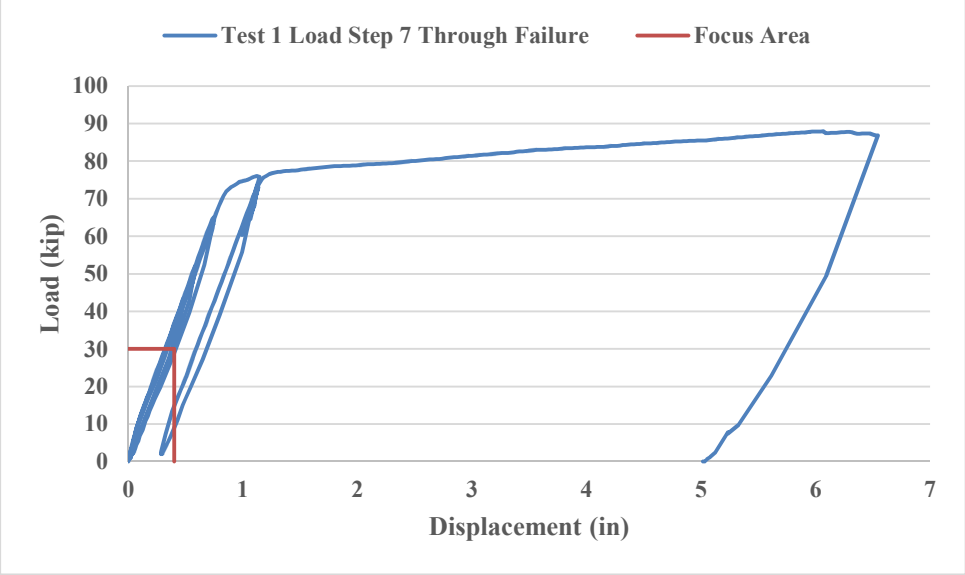

Figure 4.3 Test 1 load vs displacement curve

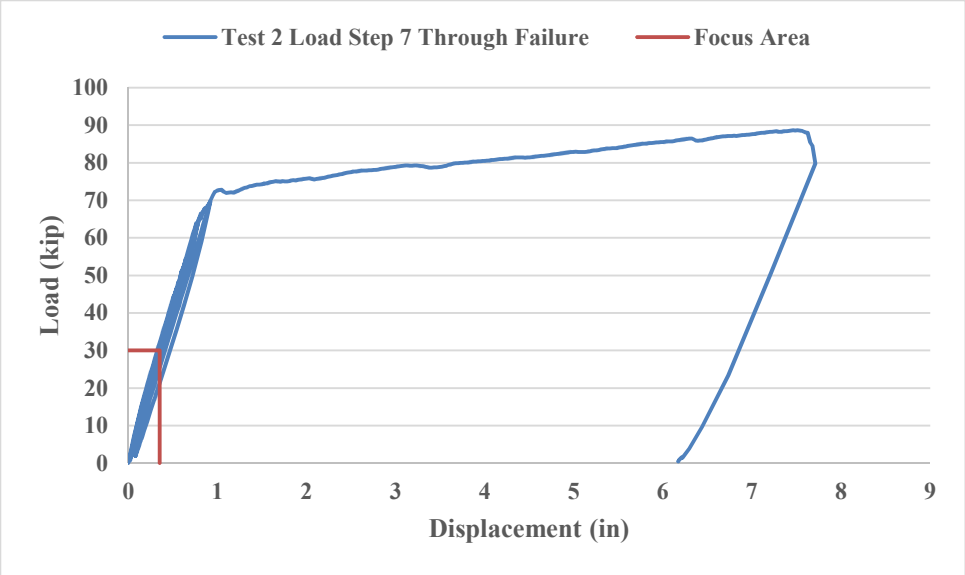

Figure 4.4 Test 2 load vs displacement curve

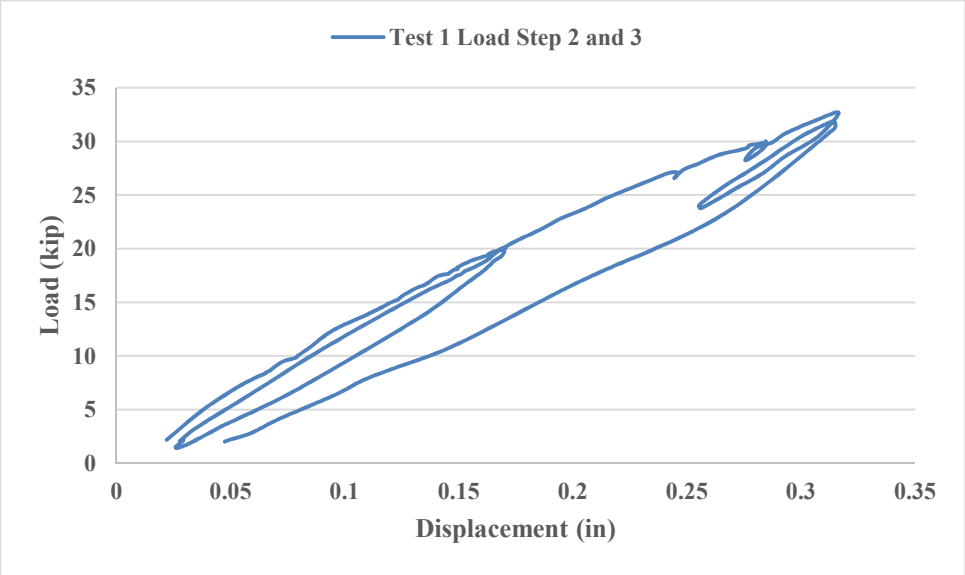

Figure 4.5 Test 1 load vs displacement curve L2 & L3

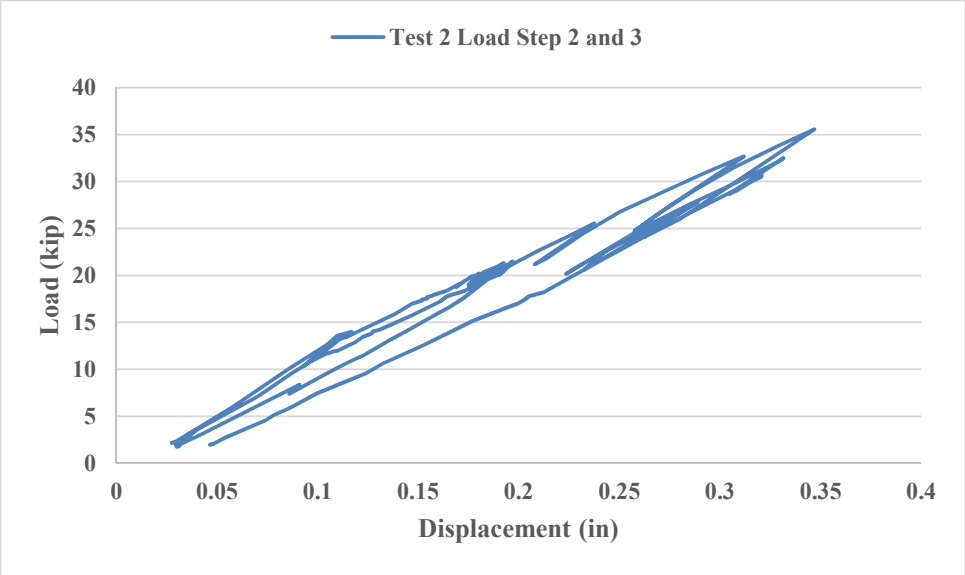

Figure 4.6 Test 2 load vs displacement curve L2 & L3

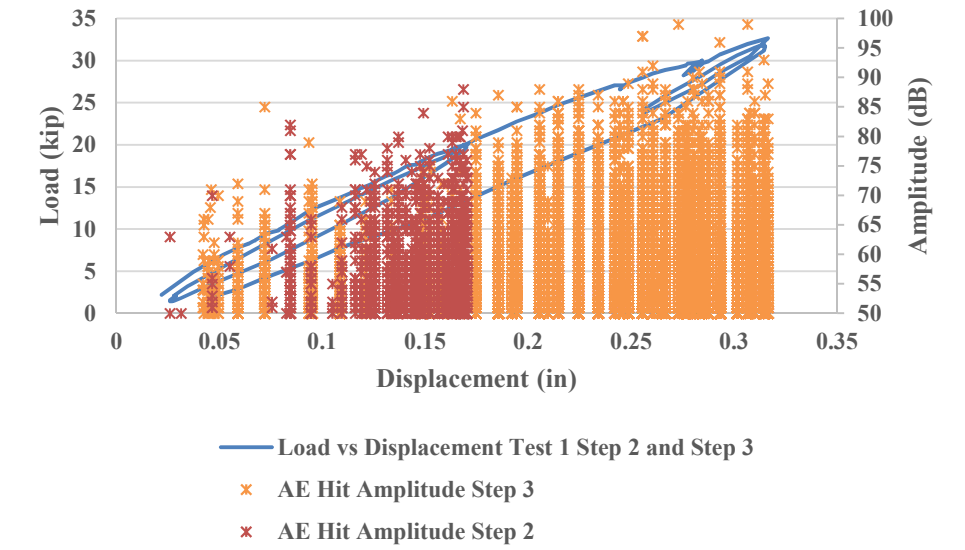

Figure 4.7 Test 1 load vs displacement w/ AE amplitude overlay

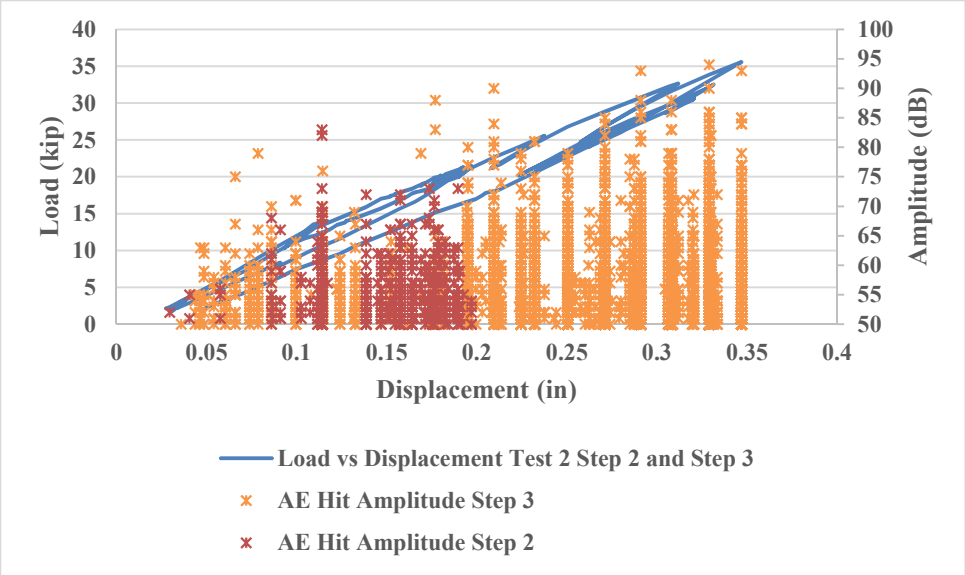

Figure 4.8 Test 2 load vs displacement w/ AE amplitude overlay

Figure 4.9 Photos of damage of T1

Figure 4.10 Photos of damage of T2

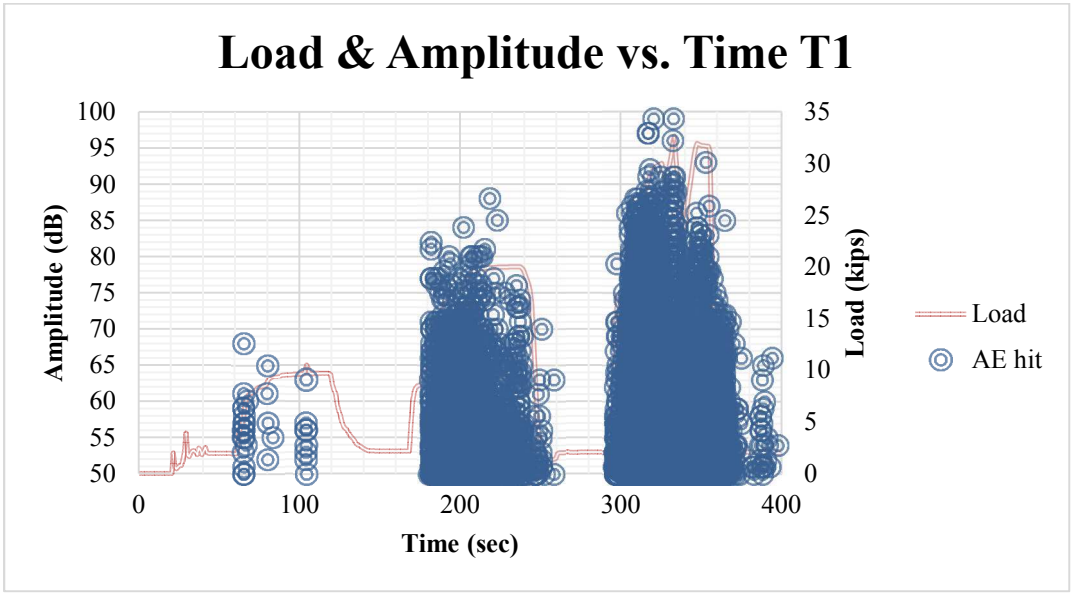

Figure 4.11 Load & amplitude vs time for T1

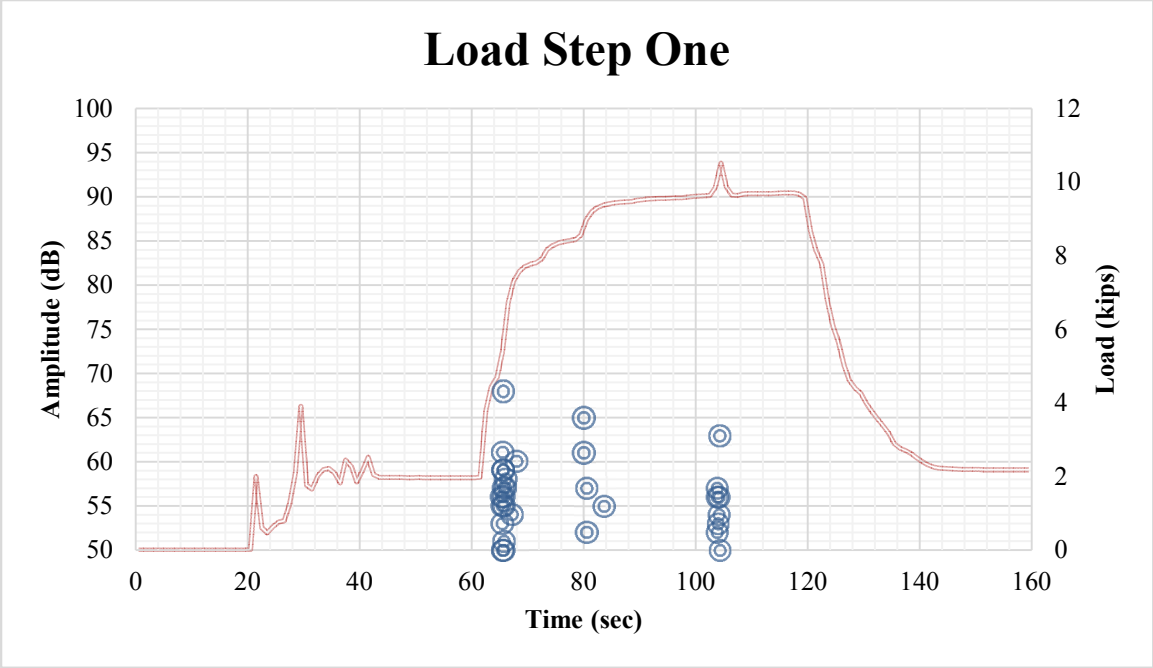

Figure 4.12 Load & amplitude vs time for T1L1

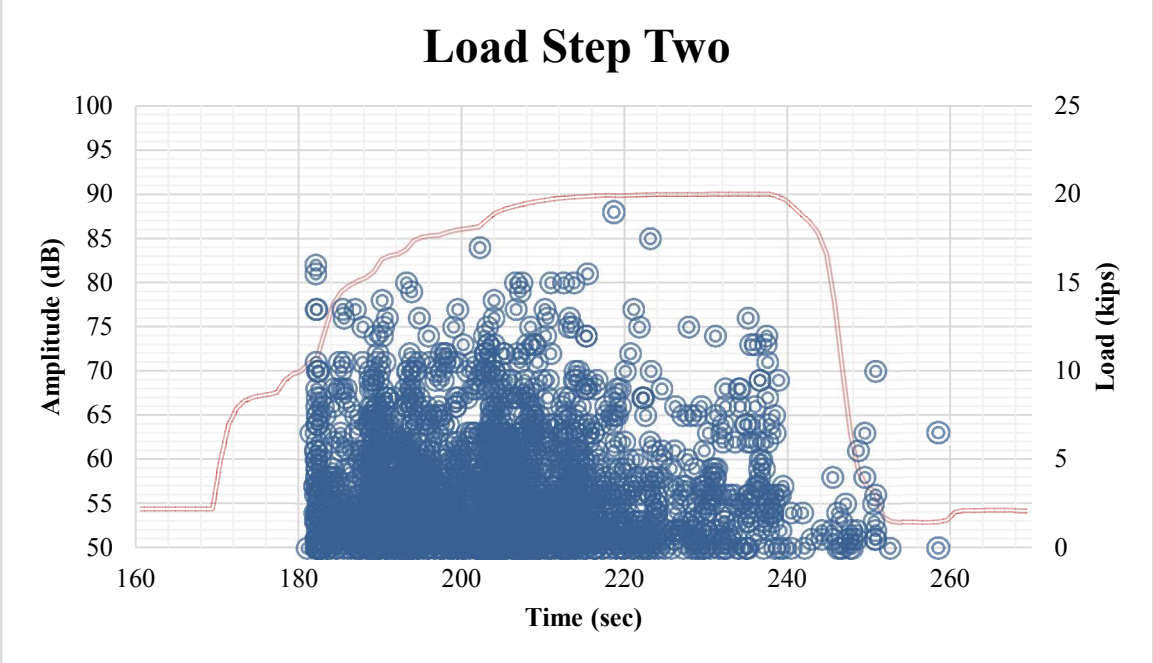

Figure 4.13 Load & amplitude vs time for T1L2

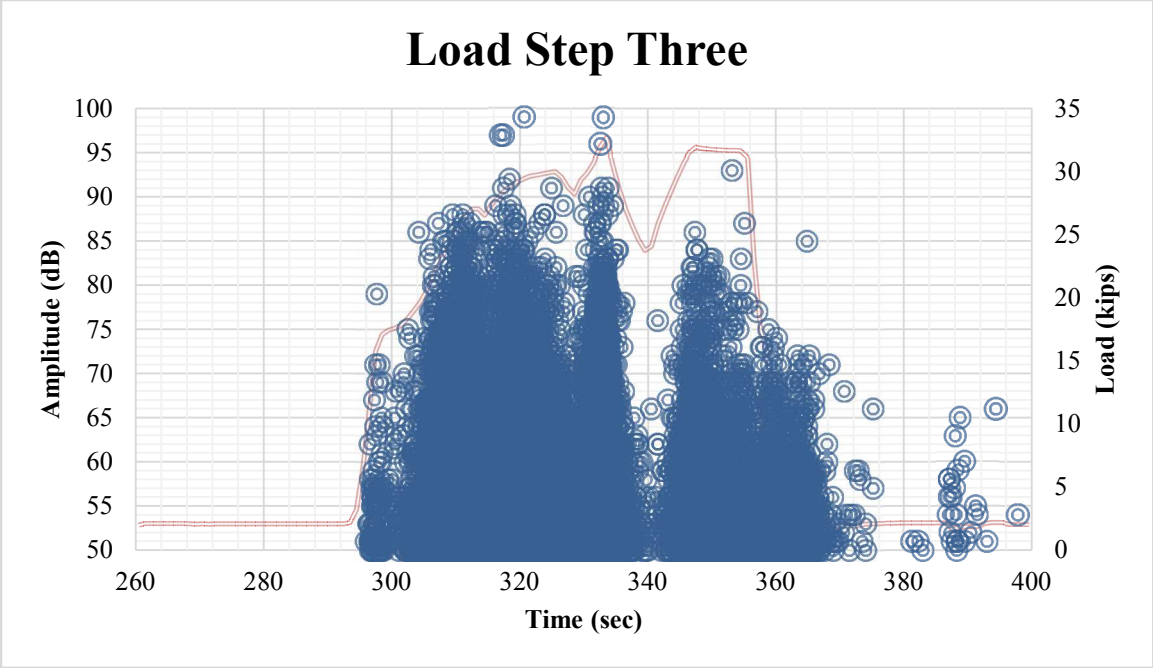

Figure 4.14 Load & amplitude vs time for T1L3

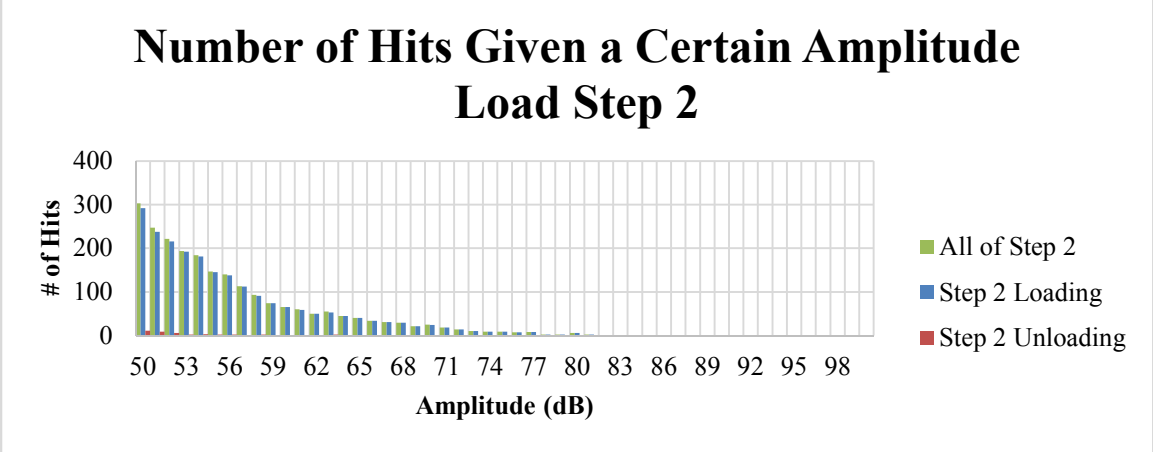

Figure 4.15 Amplitude frequencies for T1L2

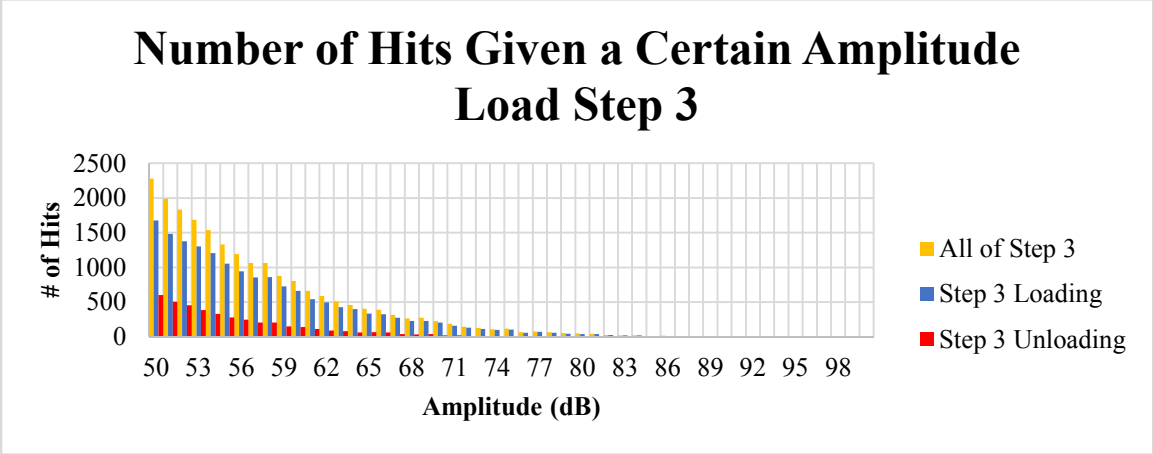

Figure 4.16 Amplitude frequencies for T1L3

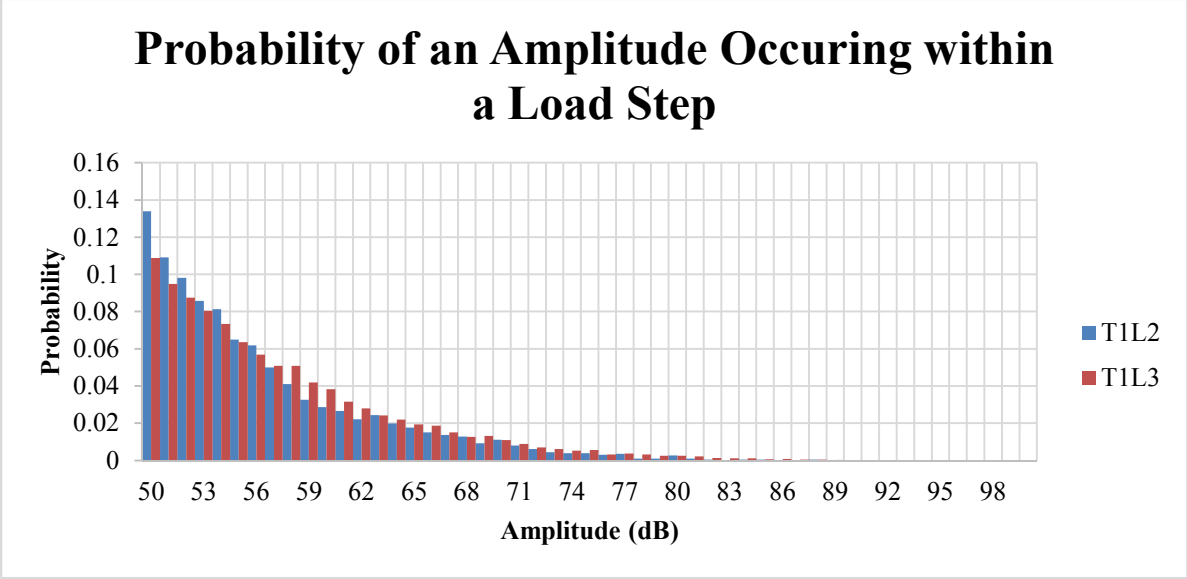

Figure 4.17 Amplitude probabilities for T1L2 & T1L3

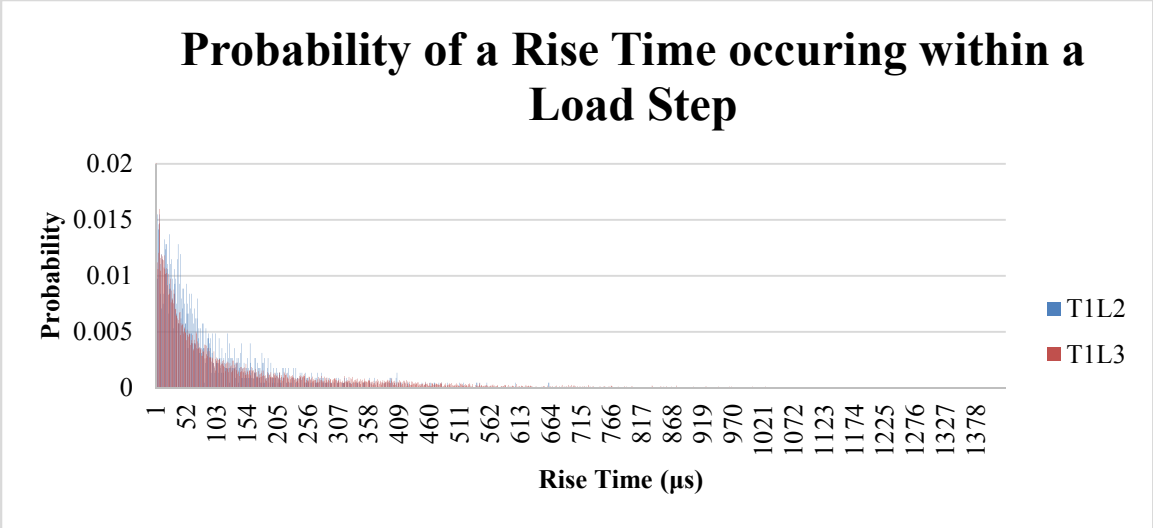

Figure 4.18 Rise time probabilities for T1L2 & T1L3

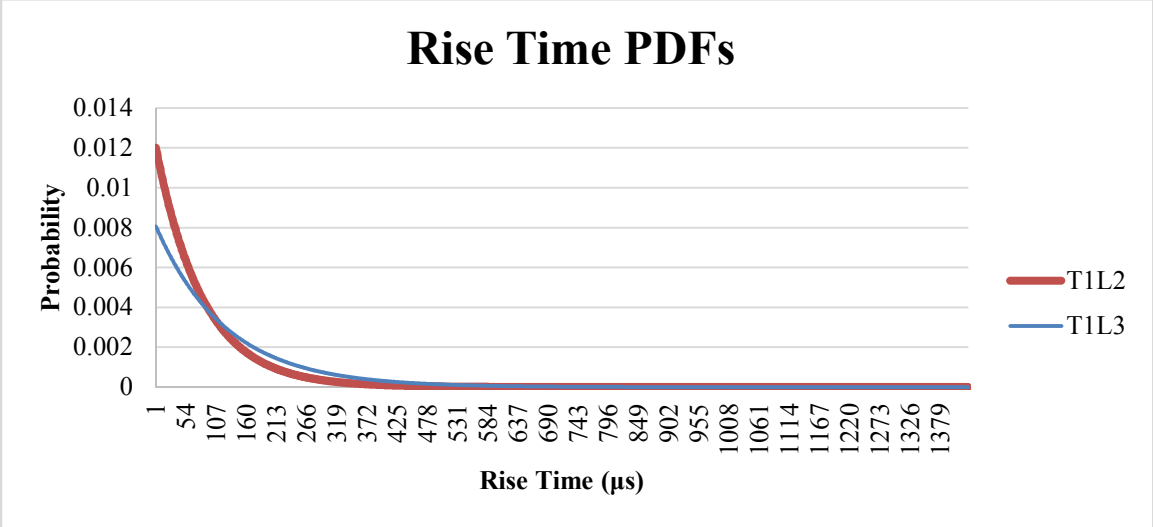

Figure 4.19 Rise time PDFs for T1L2 & T1L3

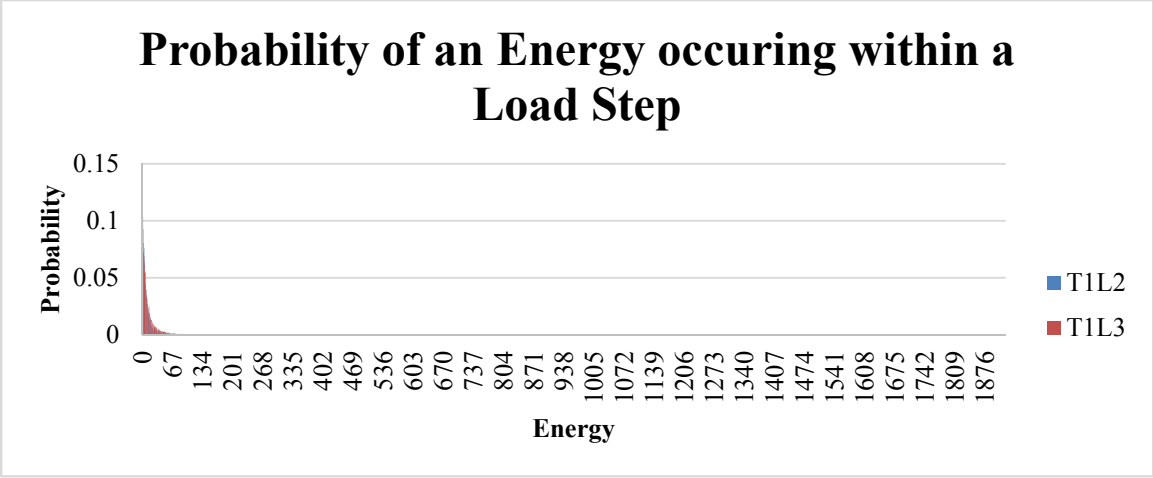

Figure 4.20 Energy probabilities for T1L2 & T1L3

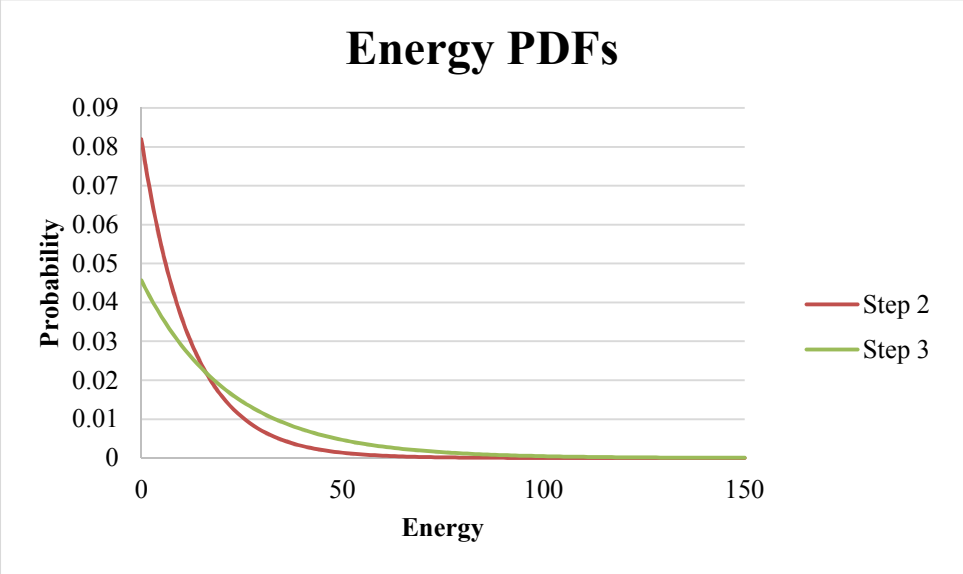

Figure 4.21 Energy PDFs for T1L2 & T1L3

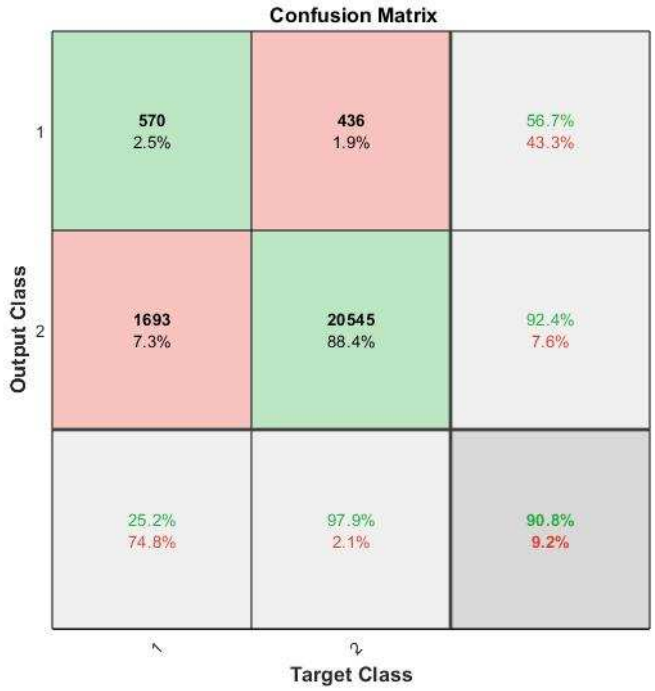

Figure 4.22 Confusion matrix of imbalanced training

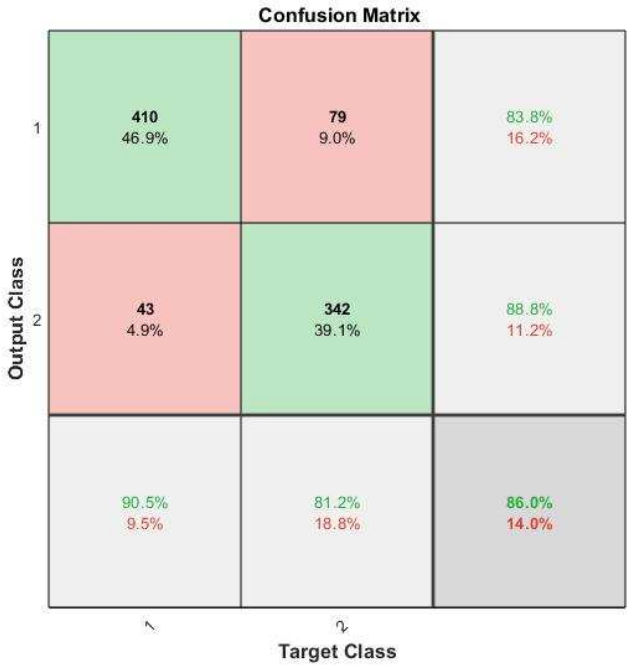

Figure 4.23 Confusion matrix of balanced training

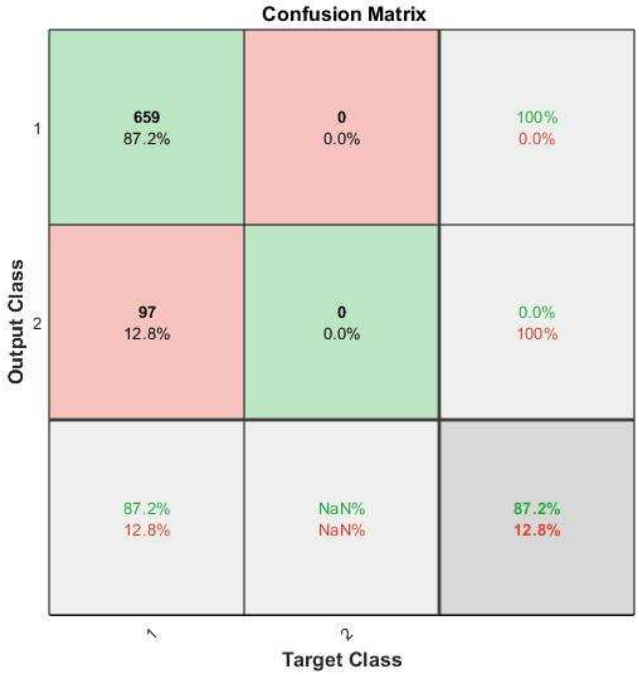

Figure 4.24 Confusion matrix of MT1 trained T2L2 tested

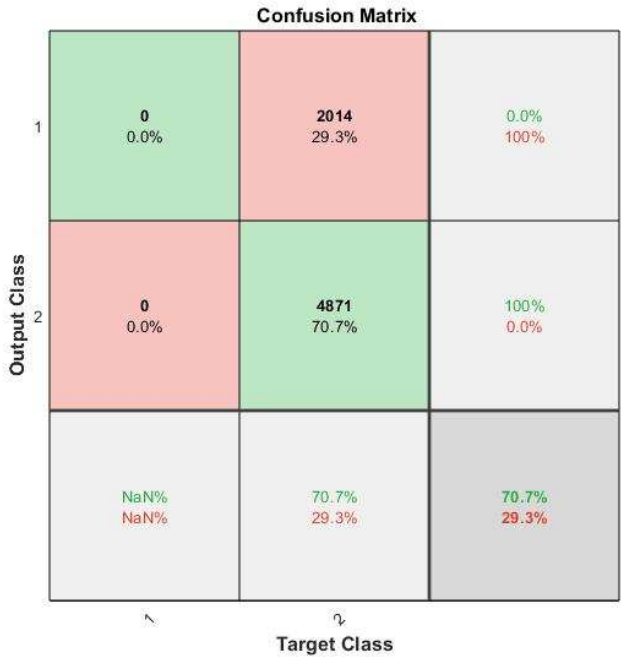

Figure 4.25 Confusion matrix of MT1 trained T2L3 tested

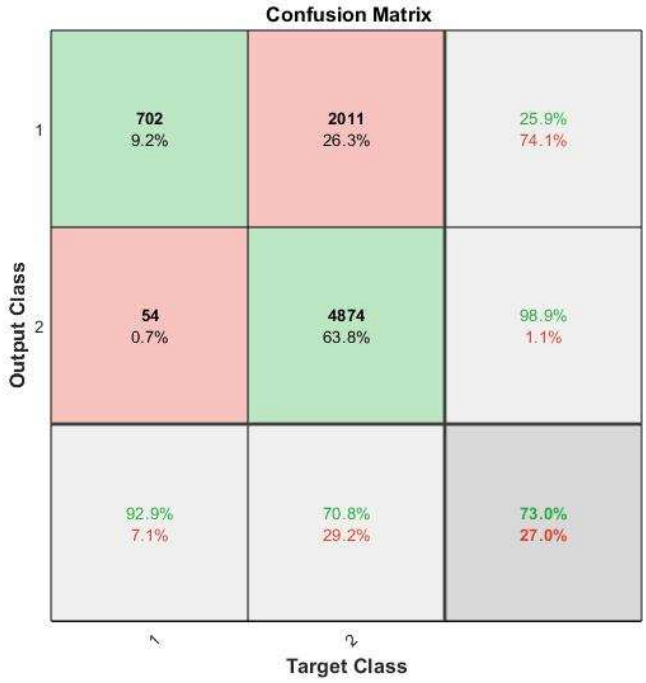

Figure 4.26 Confusion matrix of MT1 trained T2 tested

CHAPTER 5

CONCLUSION

Concluding remarks for the sections of this thesis are presented in the following chapter.

5.1 Summary

This body of work analyzed and classified AE data based on the load step in which the data was collected. The AE data was collected from flexural tests of two 15-foot concrete flat slabs. Over 30,000 hits were utilized for this study. The first analysis conducted was a statistical analysis of a single attribute of the waveforms. There were some significant differences between load steps, however the probability density and frequency charts looked very similar. The next method of analysis and classification was developing an algorithm that utilized an artificial neural network to classify the hits using the differences of all 13 features instead of 1. The idea prompting this method being that the small variances of the 13 features would allow the system to accurately classify the data points. The model was successful in classifying AE hits into load steps. Discussion on the data, as well as concluding remarks, is presented in this Chapter.

5.2 Single Attribute Analysis Conclusion

The values for each of the features analyzed were greater for the higher load step, which was expected. Each of the features analyzed has been known to increase with an

increase of intensity of damage to the structure such that the damage caused by the 30 kips should be more intense than that of 20 kips. Despite the statistical differences, the probability charts were very similar for each feature. This may be due to the sample size of the data or that there is not as significant a difference in AE data between the load steps.

The main takeaway from the single attribute analysis is that it is difficult to extract meaningful differences based on the statistics of a single AE waveform attribute largely due to the similarities of data points. That said, there are differences in the data that may be exploited given the proper statistical analysis. As it relates to SHM, prediction and classification based on a single AE attribute may not be the ideal method.

5.3 ANN Conclusion

The goal of the ANN was to classify AE hits into the load steps at which they were collected. The initial test showed the need for a balanced training method in order to accurately classify both load steps. The balanced ensemble showed the ability for accurate classification of AE hits based on the 13 features. The classification test using T2 data showed the ability of the ANN model to accurately classify unfamiliar data. This is a preliminary study so the accuracy of a well performing model has yet to be set.

It is important to note that the optimization of a neural network is an iterative process and this study introduces a method that resulted in a more balanced performance of the ANN. This thesis was able to overcome the imbalance of testing data by creating an ANN ensemble and was able to create a model with an overall classification accuracy of 86.0%. This thesis also showed the ability for an ANN to classify data from an entirely different test with an overall accuracy of 73.0%.

The main takeaways from the ANN analysis are:

- A balanced neural network ensemble proved to be more accurate at classifying both load steps
- The balanced ensemble was able to accurately classify data from an entirely different test
- Overall, an ANN is an effective tool in the classification of AE data into load steps

5.4 Recommendations for Future Work

There are many more studies that need to be conducted for this to be a viable method for the classification of AE data.

Studies must be done on similar slabs from different locations. The first and most important improvement to this study is the need for more AE data. This will allow for the ANN to have a diverse set of training and validation data which is expected to improve the accuracy of classification of unfamiliar data.

Studies must be done with more load steps and smaller step sizes. Because the goal is to be able to predict the vehicle's weight based on the AE data collected, the load steps must be smaller than 10 kips. A 10-kip range of weight is not accurate enough for the SHM field. The model would be much more accurate using 1-kip load steps.

Studies must be done on other typical structures. AE is dependent upon the mechanical properties of the surface the transducers are attached to. The current study and neural

network developed would only work for 15’ concrete flat slabs, however, the methodology would be the same.

Studies must be done on the optimization of the ANN. The neural network did not have perfect accuracy. Many articles stress the importance of the optimization of the ANN structure to provide the most accurate model. While some modification was made to the architecture of the model, many iterations or innovations can be made to optimize the network.

REFERENCES

AASHTO (2017). Bridge design specifications. American Association of State Highway and Transportation Officials, AASHTO: Washington, DC, USA.

Ai, L., Soltangharaei, V., Bayat, M., Greer, B., & Ziehl, P. (2021). Source localization on large-scale canisters for used nuclear fuel storage using optimal number of acoustic emission sensors. *Nuclear Engineering and Design*, *375*. https://doi.org/10.1016/j.nucengdes.2021.111097

Ai, L., Soltangharaei, V., Bayat, M., van Tooren, M., & Ziehl, P. (2021). Detection of impact on aircraft composite structure using machine learning techniques. *Measurement Science and Technology*, *32*(8). https://doi.org/10.1088/1361-6501/abe790

Alwosheel, A., van Cranenburgh, S., & Chorus, C. G. (2018). Is your dataset big enough? Sample size requirements when using artificial neural networks for discrete choice analysis. *Journal of Choice Modelling*, *28*. https://doi.org/10.1016/j.jocm.2018.07.002

ASTM. (2017). ASTM D6272 Standard Test Method for Flexural Properties of Unreinforced and Reinforced Plastics and Electrical Insulating Materials by Four-Point Bending. *Annual Book of ASTM Standards*, *02*(Reapproved).

Barile, C. (2019). Innovative mechanical characterization of CFRP by using acoustic emission technique. *Engineering Fracture Mechanics*, *210*. https://doi.org/10.1016/j.engfracmech.2018.02.024

Bourchak, M., Farrow, I. R., Bond, I. P., Rowland, C. W., & Menan, F. (2007). Acoustic emission energy as a fatigue damage parameter for CFRP composites. *International Journal of Fatigue*, *29*(3). https://doi.org/10.1016/j.ijfatigue.2006.05.009

Brownjohn, J. M. W. (2007). Structural health monitoring of civil infrastructure. *Philosophical Transactions of the Royal Society A: Mathematical, Physical and Engineering Sciences*, *365*(1851). https://doi.org/10.1098/rsta.2006.1925

Dundar, M. A., Ayorinde, E., & Al-Zubi, M. (2015). Determination of impact behavior of ABS from acoustic emission, ultrasound and optics. *ASME International Mechanical Engineering Congress and Exposition, Proceedings (IMECE)*, *9–2015*. https://doi.org/10.1115/IMECE2015-52948

Gifford, J. L. (1984). The innovation of the interstate highway system. *Transportation Research Part A: General*, *18*(4). https://doi.org/10.1016/0191-2607(84)90170-5

Hadzor, T. J., Barnes, R. W., Ziehl, P. H., Xu, J., & Schindler, A. K. (2011). Development of Acoustic Emission Evaluation Method for Repaired Prestressed Concrete Bridge Girders. *Research Report*, *1*.

Hassan Ali, Y., Abd Rahman, R., & Raja Hamzah, R. I. (2014). Acoustic emission signal analysis and artificial intelligence techniques in machine condition monitoring and fault diagnosis: A review. *Jurnal Teknologi (Sciences and Engineering)*, *69*(2). https://doi.org/10.11113/jt.v69.3121

Kavzoglu, T. (2009). Increasing the accuracy of neural network classification using refined training data. *Environmental Modelling and Software*, *24*(7). https://doi.org/10.1016/j.envsoft.2008.11.012

Kouroussis, D., Anastassopoulos, A., & Vionis, P. (2000). Unsupervised pattern recognition of acoustic emission from full scale testing of a wind turbine blade. *Journal of Acoustic*.

Ma, G., & Du, Q. (2020). Structural health evaluation of the prestressed concrete using advanced acoustic emission (AE) parameters. *Construction and Building Materials*, *250*. https://doi.org/10.1016/j.conbuildmat.2020.118860

Noorsuhada, M. N., Soffian Noor, M. N., Siti Norfahanim, A. M., Mohd Hisbany, M. H., & Norfaridah, M. (2019). Acoustic emission signals of pull-off test for concrete slab strengthened with cfrp using various surface preparations. *Key Engineering Materials*, *821 KEM*. https://doi.org/10.4028/www.scientific.net/KEM.821.479

Pollock, A. A. (1973). Acoustic emission - 2. Acoustic emission amplitudes. *Non-Destructive Testing*, *6*(5). https://doi.org/10.1016/0029-1021(73)90074-1

Prem, P. R., Verma, M., Murthy, A. R., & Ambily, P. S. (2021). Smart monitoring of strengthened beams made of ultrahigh performance concrete using integrated and nonintegrated acoustic emission approach. *Structural Control and Health Monitoring*, *28*(5). https://doi.org/10.1002/stc.2704

Radiuk, P. M. (2018). Impact of Training Set Batch Size on the Performance of Convolutional Neural Networks for Diverse Datasets. *Information Technology and Management Science*, *20*(1). https://doi.org/10.1515/itms-2017-0003

Ridge, A. R., & Ziehl, P. H. (2006). Evaluation of stengthened reinforced concrete beams: Cyclic load test and acoustic emission methods. *ACI Structural Journal*, *103*(6).

Saxena, A., & Saad, A. (2006). Genetic algorithms for artificial neural net-based condition monitoring system design for rotating mechanical systems. *Advances in Soft Computing*, *34*. https://doi.org/10.1007/3-540-31662-0_11

Scruby, C. B. (1987). An introduction to acoustic emission. *Journal of Physics E: Scientific Instruments*, *20*(8). https://doi.org/10.1088/0022-3735/20/8/001

South Carolina: ASCE's 2021 infrastructure report card. ASCE's 2021 Infrastructure Report Card |. (2021, September 13). Retrieved March 11, 2022, from https://infrastructurereportcard.org/state-item/south-carolina/

Stone, D. E. W., & Dingwall, P. F. (1977). Acoustic emission parameters and their interpretation. *NDT International*, *10*(2). https://doi.org/10.1016/0308-9126(77)90079-7

Tong, F., & Liu, X. (2005). Samples selection for artificial neural network training in preliminary structural design. *Tsinghua Science and Technology*, *10*(2). https://doi.org/10.1016/S1007-0214(05)70060-2

Wang, Z., Willett, P., Deaguiar, P. R., & Webster, J. (2001). Neural network detection of grinding burn from acoustic emission. *International Journal of Machine Tools and Manufacture*, *41*(2). https://doi.org/10.1016/S0890-6955(00)00057-2

Yang, B. L., & Yan, X. (2009). Identification of damage mechanisms in self-reinforced polyethylene composites by using pattern recognition techniques on AE data.

Nondestructive Testing and Evaluation, *24*(3). https://doi.org/10.1080/10589750802195477

Yang, S., & Browne, A. (2004). Neural network ensembles: combining multiple models for enhanced performance using a multistage approach. *Expert Systems*, *21*(5). https://doi.org/10.1111/j.1468-0394.2004.00285.x

Yegnanarayana, B. (2006). *Artificial Neural Networks*. Prentice-Hall of India.

Zdunek, A., Konopacka, D., & Jesionkowska, K. (2010). Crispness and crunchiness judgment of apples based on contact acoustic emission. *Journal of Texture Studies*, *41*(1). https://doi.org/10.1111/j.1745-4603.2009.00214.x